

# A *Spitzer Space Telescope* study of disks in the young $\sigma$ Orionis cluster

Jesús Hernández<sup>1,2</sup>, L. Hartmann<sup>1</sup>, T. Megeath<sup>3</sup>, R. Gutermuth<sup>4</sup>, J. Muzerolle<sup>5</sup>, N. Calvet<sup>1</sup>, A. K. Vivas<sup>2</sup>, C. Briceño<sup>2</sup>, L. Allen<sup>4</sup>, J. Stauffer<sup>6</sup>, E. Young<sup>5</sup> and G. Fazio<sup>4</sup>

hernandj@umich.edu

## ABSTRACT

We report new *Spitzer Space Telescope* observations from the IRAC and MIPS instruments of the young ( $\sim 3$  Myr)  $\sigma$  Orionis cluster. The populous nature of this cluster makes it a good target for statistically-significant studies of disk emission as a function of mass. We identify 336 stars as members of the cluster using optical and near-infrared color magnitude diagrams. Using the spectral energy distribution (SED) slopes in the IRAC spectral range, we place objects in several classes: non-excess stars, stars with optically thick disks (like classical T Tauri stars), class I (protostellar) candidates, and stars with “evolved disks”; the last exhibit smaller IRAC excesses than optically thick disk systems. In general, this classification agrees with the location expected in IRAC-MIPS color-color diagrams for these objects. We find that the evolved disk systems are mostly a combination of objects with optically thick but non-flared disks, suggesting grain growth and/or settling, and transition disks, systems in which the inner disk is partially or fully cleared of small dust. In all, we identify 7 transition disk candidates and 3 possible debris disk systems. There appears to be a spatial extension of infrared excess sources to the north-east, which may be associated with the young ( $< 1$  Myr) embedded cluster NGC 2024. As in other young stellar populations, the fraction of disks depends on the stellar mass, ranging from  $\sim 10\%$

---

<sup>1</sup>Department of Astronomy, University of Michigan, 830 Dennison Building, 500 Church Street, Ann Arbor, MI 48109, US

<sup>2</sup>Centro de Investigaciones de Astronomía, Apdo. Postal 264, Mérida 5101-A, Venezuela.

<sup>3</sup>Ritter Observatory, MS 113, Department of Physics and Astronomy, University of Toledo, OH 43606-3390.

<sup>4</sup>Harvard-Smithsonian Center for Astrophysics, 60 Cambridge, MA 02138, US

<sup>5</sup>Steward Observatory, University of Arizona, 933 North Cherry Avenue, Tucson, AZ 85721, US

<sup>6</sup>*Spitzer* Science Center, Caltech M/S 220-6, 1200 East California Boulevard, Pasadena, CA 91125

for stars in the Herbig Ae/Be mass range ( $>2 M_{\odot}$ ) to  $\sim 35\%$  in the T Tauri mass range ( $1-0.1 M_{\odot}$ ). We find that the disk fraction does not decrease significantly toward the brown dwarf candidates ( $<0.1 M_{\odot}$ ). The IRAC infrared excesses found in stellar clusters and associations with and without central high mass stars are similar, suggesting that external photoevaporation is not very important in many clusters. Finally, we find no correlation between the X-ray luminosity and the disk infrared excess, suggesting that the X-rays are not strongly affected by disk accretion.

*Subject headings:* infrared: stars: formation — stars: pre-main sequence — open cluster and associations: individual ( $\sigma$  Orionis cluster) — protoplanetary systems: protoplanetary disk

## 1. Introduction

Observations have shown and theory predicts that disks around young stars are an inescapable consequence of star formation, given angular momentum conservation during protostellar cloud core collapse (Hartmann 2005a; Ward-Thompson et al. 2005; Andre et al. 2000). As the resulting protoplanetary disks age, their excesses at near-infrared (NIR) and mid-infrared wavelengths decrease. Previous studies have indicated that the timescale for this evolution in disk emission is strongly dependent on the stellar mass (Lada & Lada 1995; Muzerolle et al. 2003; Calvet et al. 2004; Sicilia-Aguilar et al. 2005) ranging from 5-7 Myr for objects in the mass range of the T Tauri stars (TTS, with spectral type K5 or later; Haisch et al. 2001; Hartmann 2005b; Hillenbrand et al. 2006) to  $<3$  Myr for objects in the mass range of the Herbig Ae/Be (HAeBe) stars (spectral type F5 or earlier; Hernández et al. 2005).

The observed decreases in infrared emission can result from: grain growth to sizes much larger than the wavelength of observation; dust settling to the disk midplane, which reduces the “flaring” of the disk and thus the amount of energy radiated (Kenyon & Hartmann 1987; Dullemond & Dominik 2005; D’Alessio et al. 2006); clearing of small dust particles by large bodies in the disk; or some combination of these processes. Since grain growth and settling to the mid-plane occur fastest in the (warmer) inner disk (Weidenschilling 1997; Dullemond & Dominik 2004), the disk emission is expected to decline faster at short wavelengths than at long wavelengths, and there is observational evidence for this (Sicilia-Aguilar et al. 2006; Hartmann 2005b; Lada et al. 2006).

Of particular interest are “transition disk” objects, which have an inner, optically thin

disk region, possibly produced by planet clearing, combined with an outer, optically thick disk (Calvet et al. 2002, 2005; D’Alessio et al. 2005a; Megeath et al. 2005a). Prior to the complete or nearly-complete clearing seen in transition disks, one would expect to observe optically-thick but reduced infrared emission from the inner disk, for which there is some evidence (e.g., Sicilia-Aguilar et al. 2006; Lada et al. 2006). However, additional large samples of stars are desirable to make the result more statistically significant, as stars of the same mass and age show a wide range of disk emission properties (Furlan et al. 2006).

The  $\sigma$  Orionis cluster is of particular interest because it is reasonably near and relatively populous, making possible statistically-significant studies of disk properties as a function of stellar mass. Moreover,  $\sigma$  Orionis has an age  $\sim 3$  Myr at which one might expect the beginnings of disk evolution to become evident. It is part of the Orion OB1b sub-association which has an age of 1.7-7 Myr (Warren & Hesser 1978; Brown et al. 1994, 1998; Briceño et al. 2005). Low-mass members of the  $\sigma$  Orionis cluster were first reported by Walter et al. (1997), who found over 80 X-ray sources and spectroscopically identified more than 100 low mass, pre-main sequence (PMS) members lying within 1 degree from the star  $\sigma$  Ori. The distance calculated by Hipparcos for this star ( $352_{-85}^{+166}$ ) agrees, within the uncertainties of Hipparcos, with the Hipparcos distance calculated for the overall population of the stellar subassociation OB1b ( $439 \pm 33$ ; Brown et al. 1998), which is statistically more reliable. The estimated age of the cluster is 2-4 Myr (Zapatero Osorio et al. 2002; Oliveira et al. 2002; Sherry et al. 2004; Franciosini et al. 2006). Since the  $\sigma$  Orionis cluster is relatively near and the reddening toward the center of the cluster is low ( $E(B-V)=0.05$  mag; Brown et al. 1994; Béjar et al. 1999), this stellar cluster is an excellent laboratory to study young stars in a entire range of mass, from the massive and multiple O9.5 type star  $\sigma$  Ori to the lowest mass objects, like brown dwarfs and free-floating planets (e.g., Barrado y Navascués et al. 2001, 2003; Béjar et al. 1999, 2001, 2004; Burningham et al. 2005; Caballero 2005; Kenyon et al. 2005; Oliveira et al. 2006; Scholz & Eisloffel 2004; Sherry et al. 2004; Zapatero Osorio et al. 2002; Walter et al. 1998).

The unprecedented sensitivity and spatial resolution provided by the *Spitzer Space Telescope* in the near- and mid-infrared windows are powerful tools to expand significantly our understanding of star and planet formation processes. In this contribution, we analyze the near- and mid-infrared properties of stars in the  $\sigma$  Orionis cluster, ranging in mass from HAeBe stars to the substellar limit.

This paper is organized as follows. In §2 we present the observational data. In §3 we describe the selection of cluster members. We analyze the observations and describe the results on §4, and give our conclusions in §5.

## 2. Observations

### 2.1. Infrared photometry

We have observed a field of  $\sim 1730$  arcmin<sup>2</sup> on the  $\sigma$  Orionis cluster using the four channels (3.6, 4.5, 5.8, and 8.0  $\mu$ m) of the InfraRed Array Camera (IRAC, Fazio et al. 2004); 90% of this field was also observed using the 24  $\mu$ m band of the Multiband Imaging Spectrometer for *Spitzer* (MIPS, Rieke et al. 2004).

The IRAC observations presented here were taken on October 9, 2004. The field of view was covered by a  $9 \times 10$  position mosaic (20" overlap), with three dithered exposures at each position. Images were obtained in High Dynamic Range (HDR) mode, whereby a short integration (1 second) is immediately followed by a long integration (26.8 seconds). Standard Basic Calibrated Data (BCD) products from version S13.2 of the *Spitzer* Science Center's IRAC pipeline were used to make the final mosaics. Post-BCD data treatment was performed using custom IDL software (Gutermuth et al. 2004, Gutermuth et al. 2006) that includes modules for detection and correction of bright source artifacts, detection and removal of cosmic ray hits, construction of the long and short exposure HDR mosaics, and the merger of those mosaics to yield the final science images.

MIPS observations were made using the medium scan mode with half-array cross scan overlap, resulting in a total effective exposure time of 80 seconds. The 24  $\mu$ m images were processed using the MIPS instrument team Data Analysis Tool (DAT), which calibrates the data and applies a distortion correction to each individual exposure before combining into a final mosaic (Gordon et al. 2005).

Figures 1 and 2 show the IRAC color and the MIPS 24  $\mu$ m images of the  $\sigma$  Orionis cluster. The lower-right panel in Figure 2 shows a map of dust infrared emission (Schlegel et al. 1998) illustrating the location of the cluster in the OB1b sub-association, which can be traced by the ringlike structure centering at RA $\sim$ 84 and DEC $\sim$ -2 (Briceño et al. 2005; Hernandez et al. 2006). In this panel, the boxes show the positions of the IRAC (small box) and MIPS (large box) scan regions. The isocontours are estimators of galactic extinction (for  $A_V=0.2, 0.4, 0.6$  &  $0.8$  mag) from the 100  $\mu$ m map of dust emission (see, Schlegel et al. 1998). The galactic extinction and the background at 8 and 24  $\mu$ m is quite low compared with other regions with similar ages, which improves the precision and sensitivity of the photometry.

Point source detections were carried out individually on each IRAC band using PhotVis (version 1.09), an IDL GUI-based photometry visualization tool developed by R. Gutermuth using the DAOPHOT modules ported to IDL as part of the IDL Astronomy User Library

(Landsman 1993). More than 10,000 sources were detected in at least one *Spitzer* band. We extracted the photometry of these objects using the *apphot* package in IRAF, with an aperture radius of  $3''.7$  and a background annulus from  $3.7$  to  $8''.6$ . We adopted zero-point magnitudes for the standard aperture radius ( $12''$ ) and background annulus ( $12$ - $22''.4$ ) of 19.665, 18.928, 16.847 and 17.391 in the [3.6], [4.5], [5.8] and [8.0] bands, respectively. Aperture corrections were made using the values described in IRAC Data Handbook (Reach et al. 2006). A preliminary list of 1682 objects (hereafter *Sample 1*) was created by selecting those objects having photometric measurements in all IRAC bands with errors less than 0.15 magnitudes. We obtained point source photometry at  $24\ \mu\text{m}$  with IRAF/*daophot* point spread function fitting, using an aperture size of about  $5''.7$  and an aperture correction factor of 1.73 derived from the STinyTim PSF model. The absolute flux calibration uncertainty should be 4% (Engelbracht et al. 2006). Because of the contamination by the bright star  $\sigma$  Ori in the IRAC and MIPS images, stars located within  $30''$  of this O star were not included in the preliminary list.

## 2.2. Optical photometry

Optical magnitudes were obtained from the CIDA Equatorial Variability survey which is being carried out using the QUEST I camera (Baltay et al. 2002) installed at the Jurgen Stock Telescope (a 1-m Schmidt telescope) at the Venezuelan National Observatory of Llano del Hato. The camera, an array of  $4 \times 4$  CCDs, is designed to work in driftscan mode, which is a very efficient way to survey large areas of the sky. Each scan of the sky was reduced and calibrated with the standard QUEST software and the method described in Vivas et al. (2004) for scans centered at  $\delta = -1$ . We used data from multiple scans centered at  $\delta = -3^\circ$ . The scans have a width of  $2.2^\circ$  in  $\delta$ . The range in right ascension shown in Figure 1 is covered completely by these optical observations. However, there is no data in a small region from  $-2.52^\circ < \delta < -2.44^\circ$ , corresponding to the gap between CCDs in the QUEST I camera. Most objects with an optical counterpart have more than 10 measurements, so we can identify the variables using differential photometry (Vivas et al. 2004).

## 3. Membership selection

We do not have spectroscopic confirmation for most of the probable members in the  $\sigma$  Orionis cluster. We must use photometric criteria to make a robust selection of members, as described below.

### 3.1. Rejecting extragalactic objects

Figure 3 shows the [3.6] versus [5.8]-[8.0] color-magnitude diagram for *Sample 1* (§2.1). The bulk of the sample has [5.8]-[8.0] $\sim$ 0 and [3.6] $<$ 14.5; below this limit the number of objects with photospheric colors ([5.8]-[8.0] $\sim$ 0) decreases drastically, and the contamination from extragalactic sources is expected to be more than 50% (Fazio et al. 2004). We identify extended sources (crosses) by computing the radial profile for each object using the *radprof* task in IRAF, and designate as extended sources those with FWHM values more than 3 standard deviations from the median in all IRAC bands; typically this means FWHM $>$ 2". Most objects located below the [3.6] band limiting magnitude (solid line) in Figure 3 are identified in this way as extended sources and are likely to be extragalactic objects. We therefore initially restrict our sample to objects above the solid line in Figure 3.

Some galaxies have very red colors because of strong PAH (polycyclic aromatic hydrocarbon) emission; with features at 7.7, 8.6, 11.2, 12.7, 16.4, and 17.1  $\mu$ m correlated with star formation rates (Wu et al. 2005). Gutermuth et al. (2006) showed that the [4.5 - 5.8] versus [5.8 - 8.0] and [3.6 - 5.8] versus [4.5 - 8.0] color-color diagrams can be used to eliminate most of these objects. As shown in Figure 4, objects below and to the right of the solid lines are likely to be PAH-rich galaxies. We find that most of the PAH-rich galaxy candidates have extended radial profiles as inferred from point-source fitting. Visual inspection of the IRAC images also shows that many of these candidates are diffuse objects. In addition to the galaxies, other objects with similar colors turn out to be faint companions of brighter stars, thus calling into question the accuracy of the photometry. Only one object (open square) with a stellar profile is located in the PAH-rich galaxies regions; this star (HD294268=SO411) has been identified as a young star with spectral type F5 (Gregorio-Hetem & Hetem 2002). We therefore eliminate the rest of the objects below the solid lines in Figure 4, resulting in a sample of 1280 stellar sources (hereafter *Sample 2*).

About 40% of the objects in *Sample 2* do not have optical counterparts in the CIDA Equatorial Variability survey; most of these objects are fainter than the limiting magnitude ( $V\sim$ 19.7) or brighter than the saturation limit ( $V\sim$ 13.5) of this survey. Some of the objects in *Sample 2* also are located on the gap in declination of the survey. We augmented the V optical data set using photometry from (Sherry et al. 2004) and for the brightest objects from the Kharchenko (2001) catalog.

### 3.2. Additional photometric selection

Virtually all the objects in *Sample 2* (99%) have 2MASS counterparts (Cutri et al. 2003). Figure 5 shows the distributions of J magnitudes for all 2MASS sources in the IRAC field (open histogram) and for the 2MASS sources included in *Sample 2* (striped histogram). Comparison of these two histograms indicates that *Sample 2* is essentially complete to about  $J=14.0$ . Assuming a reddening of  $E(B-V)=0.05$  (Brown et al. 1994; Béjar et al. 1999), a distance of  $D=440$  pc (Brown et al. 1998; Hernández et al. 2005) and the 3 Myr isochrones from Baraffe et al. (1998), the equivalent completeness limit in mass is  $\sim 0.15 M_{\odot}$  (spectral type  $\sim M5$ ). For comparison, the distribution of J magnitudes for our MIPS detections (solid histogram) is shown in Figure 5. Most of brightest objects ( $J<11$ ;  $\sim 1.5 M_{\odot}$ ) have  $24 \mu\text{m}$  detections.

*Sample 2* includes 214 stars previously found to be members by other investigators (hereafter previously known members; see the Appendix A). Of these objects, the membership of 104 stars were confirmed spectroscopically, while the other 110 stars were assigned membership based only on optical photometry. In addition, 105 objects in our sample have been identified as X-ray sources by Franciosini et al. (2006), of which 49 objects have not been identified previously as spectroscopic or photometric members.

Figure 6 shows the V versus V-J color-magnitude diagram for *Sample 2*. Filled squares (spectroscopic members) and filled triangles (photometric members) represent previously known members; both distributions share the same region in Figure 6 suggesting that optical photometric selection can be effective in identifying low mass members (see also; Kenyon et al. 2005; Burningham et al. 2005). The stars with  $3 < V - J < 4$  roughly follow the 3 Myr isochrone of Baraffe et al. (1998, dashed curve), while the redder stars depart significantly from the theoretical isochrone; this may be due to incompleteness in the opacity tables at low temperatures, resulting in theoretical colors that are too blue for  $V-J > 4$  (Lyra et al. 2006; Baraffe et al. 1998). Filled circles represent the higher mass stars selected by Kharchenko et al. (2004) with high membership probabilities ( $>50\%$ ); the plus symbols represent bright stars with very low probabilities of membership.

The mean of the distribution of previously known cluster members can be characterized roughly as straight line in the V versus V-J diagram, with a standard deviation  $\sigma(V-J) = 0.27$  mag. As a first approximation, we define the photometric region of probable members as the region above the dotted line in Figure 6. This line represents the lower  $3 \sigma$  deviation from the mean distribution line. The X-ray detected stars (Franciosini et al. 2006), labeled by open squares, are mostly located in the region of the previously known cluster members (most of these objects were identified previously as cluster members). Therefore, X-ray emission can be used as an additional criterion supporting membership in young stellar groups (e.g.;

Carkner et al. 1998; Preibisch & Feigelson 2005; Franciosini et al. 2006).

Figure 7 shows the J versus J-K color-magnitude diagram for *Sample 2*. Stars with  $J > 11.5$  have similar J-K colors, in agreement with the trend expected for the 3 Myr isochrone from Baraffe et al. (1998). For these stars, the distribution of J-K color can be represented as a Gaussian function centered at  $J-K=0.94$  with  $\sigma(J-K) = 0.06$ . We adopt the border between members and non-members to be the  $3\sigma$  deviation line (dotted line). For stars with  $J < 11.5$ , we define the region of probable members by using the X-ray sources in addition to the known members of the cluster. The crosses represent non-members defined using Figure 6 (below the dotted line). Some of these non-members, with  $J > 13$ , appear in the region of probable members in Figure 7, so some contamination would result from selecting stars using 2MASS colors alone.

Our preliminary member sample consists of stars located redward from dotted lines in Figures 6 and 7, X-ray sources (Franciosini et al. 2006), and previously known members (see §A) located redward from the dotted line in Figure 7. Our preliminary uncertain member sample of the cluster includes those objects selected using only the criterion defined in Figure 7, where the contamination of non-members could be important and additional confirmation is required.

The most important source of contamination are field M dwarfs. Given the galactic latitude of the  $\sigma$  Orionis cluster ( $b \sim 17.3$  deg), M giant stars are not expected to be a significant source of contamination ( $< 5\%$ ) in the cluster (Béjar et al. 1999, 2004). We identify 3 possible M giants stars using the J-H versus H-K color-color diagram (Bessell & Brett 1988), including them in the uncertain members sample.

Jeffries et al. (2006) showed that young stars located in the general region of the cluster consist of two populations with different mean ages and distances superimposed along the line of sight: one with an age of 3 Myr located at 439 pc (consistent with the  $\sigma$  Orionis cluster) and the other with 10 Myr located at 326 pc, which could be associated with the Orion OB1a association (Jeffries et al. 2006; Briceño et al. 2006). However, most of the objects belonging to the older stellar group are located north-ward from the main population of  $\sigma$  Orionis cluster, so that the contamination by the older stars in our survey should be small,  $\lesssim 10\%$  (Jeffries 2006, private communication). In particular, 11 out of 75 stars included in our preliminary member sample have radial velocities from Jeffries et al. (2006) consistent for stars in the older population but inconsistent with those of the  $\sigma$  Orionis cluster. These stars were included, with a note, in the uncertain member sample. Only two stars in our uncertain members sample have radial velocity expected of stars in the  $\sigma$  Orionis cluster; we included these in our final membership list.

The final catalogs include 336 stars in the member sample and 133 stars in the uncertain member sample. In the member sample, 132 stars have optical photometry from the CIDA survey, of which 57 stars (43%) were classified as variable stars using the method described in Vivas et al. (2004); since young stars are expected to exhibit photometric variability (e.g.; Cohen & Schwartz 1976; Herbst & Shevchenko 1999; Briceño et al. 2005), this is an additional criterion supporting membership.

Table 1 shows IRAC, MIPS and V photometry data for stars in the *member sample* according to the criteria discussed above. Column 1 shows the internal running identification number in our sample; columns 2 and 3 are the stellar coordinates; columns 4, 5, 6 and 7 give IRAC magnitudes in the bands [3.6], [4.5], [5.8] and [8.0], respectively; column 8 gives MIPS (24  $\mu\text{m}$ ) magnitudes; columns 9 and 10 show the V magnitudes and its sources; column 11 indicates if the star has been identified as variable in the CIDA survey; column 12 indicates if the star is a x-ray source (Franciosini et al. 2006); column 13 shows the disk classification based on the IRAC and MIPS analysis (see §4); the last column gives the references for the *previously known members*. Table 2 shows IRAC and MIPS photometry for stars included in the *uncertain member sample*. The information shown in this table in columns from 1 to 8 is the same as in Table 1. The last column shows the disk classification based on the IRAC and MIPS analysis discussed in the following section.

## 4. Results

### 4.1. Infrared color-color diagrams

Figure 8 shows two IRAC color-color diagrams, [5.8]-[8.0] versus [3.6]-[4.5] (left panels) and [4.5]-[5.8] versus [3.6]-[4.5] (right panels), for the members (upper panels) and uncertain members (lower panels). Different symbols show the disk classification based on the IRAC SED slope (§4.2). Particularly, triangles, squares and diamonds represent stars with different levels of infrared emission, while circles are non-excess stars. Symbols surrounded by open squares show objects with small or no excesses in the IRAC bands but large excesses at 24  $\mu\text{m}$  (see below). The dashed box in the [3.6] - [4.5] versus [5.8] - [8.0] color-color diagram indicates the region predicted for stars with optically-thick disks (§4.2) by the models of D’Alessio et al. (2005b)

The upper-left panel of Figure 8 shows that most of stars with significant IRAC excess (squares; hereafter IRAC class II stars) have colors in agreement with model colors for optically-thick disks. The stars without IRAC excesses (hereafter IRAC class III stars) are located around the photospheric region ([5.8]-[8.0] $\sim$ 0, [3.5]-[4.5] $\sim$ 0). A few systems are found

in the region between the IRAC class III and class II stars; these objects with weak IRAC excess (triangles) are discussed in more detail in §4.2. Two of these objects (the stars SO638 and SO299) have  $[3.6]-[4.5] \lesssim 0$ , while exhibiting significant emission at longer wavelengths. Three other objects (diamonds) have very large excesses which may suggest the presence of a protostellar envelope (hereafter IRAC class I candidates); SO457 (IRAS05358-0238), SO927 (an emission line object Weaver & Babcock 2004), and SO411 (HD294268). The last two objects have  $[3.6]-[4.5]$  colors expected for class II systems, so these objects are more likely to be objects with optically-thick disks and high  $8 \mu\text{m}$  fluxes due to strong silicate emission or rising SEDs at wavelength longer than  $5.8 \mu\text{m}$  (§4.3).

In the upper-right panel of Figure 8, the  $[4.5]-[5.8]$  colors of IRAC class II stars shows less scatter in comparison with the  $[5.8]-[8.0]$  colors. There may be some PAH background contamination present in the  $[8.0]$  band; however, this also could indicate that intrinsic differences in disk flaring or other properties that may be more easily detected at  $8 \mu\text{m}$  (D’Alessio et al. 2006). For example, the IRAC class II stars located redward from the dashed box (SO462, SO774 and SO1266) and the star SO411 (with  $[5.8]-[8.0] > 1.5$ ) in the upper-left panel, have a flat or rising SEDs at wavelengths longer than  $5.8 \mu\text{m}$  (see §4.3).

In the lower panels, nine IRAC class II stars are located in the region expected for stars with optically thick disks, and thus are likely to be cluster members. One IRAC class II star (SO1356), located below the model region, has an excess at  $[5.8]-[8.0]$ , but not at  $[3.6]-4.5$  or  $[4.5]-[5.8]$ . This star was not covered in the MIPS field, so it is not clear if the excess observed at  $8 \mu\text{m}$  originates from PAH background contamination or from emission from an outer disk. The object SO1293 (represented by the triangle) has a larger excess at  $[4.5]-[5.8]$  than at  $[5.8]-[8.0]$ ; it is faint ( $J=15.64$ ) and so could have a longer wavelength excess below the MIPS detection limit.

Five uncertain members with very large infrared excesses (IRAC class I candidates), are plotted in the IRAC color-color diagrams: SO950, SO336, SO361, S0916 and SO668. Because AGN are located in the same region as the class I objects in these diagrams (Stern et al. 2005) and are too faint to easily detect spatial extension, additional data are needed to confirm these objects as protostellar members.

Figure 9 shows K-[24] versus J-H color-color diagrams for members (upper panel) and uncertain members (lower panel). We sort the objects into three regions, depending upon the magnitude of their K-[24] excesses (see also Hernandez et al. 2006). One region consists of  $K-[24] < 0.5$ , corresponding to systems with undetectable or very uncertain long-wavelength excesses, given photometric errors. A second region encompasses objects with  $K-[24] > 3.3$ , corresponding to optically-thick disk emission and/or protostellar envelope emission. Finally, the intermediate-excess region  $0.5 < K-[24] < 3.3$  is consistent with colors typical of optically-

thin debris disks [the famous  $\beta$  Pic debris disk system, which is one of the debris disk system with largest  $24 \mu\text{m}$  excess known, has  $K-[24] \sim 3.3$ ; (e.g., Gorlova et al. 2004; Rieke et al. 2005)].

There are seven members with very large [24] excesses but low IRAC excesses (symbols surrounded by open squares); SO908, SO818, SO1267, SO897, SO299, SO587 and SO1268. The last object has no detectable IRAC excess. These stars are possible “transition disk” systems, in which the inner disk is completely or nearly-completely cleared of small dust but the outer disk is optically thick (Calvet et al. 2002, see §4.1). In the lower panel, the uncertain member SO120 is also a transition disk candidate.

There are two early type members which are located in the intermediate-excess region: SO913 ( $J-H=-0.04$ ) has no IRAC excess and SO956 ( $J-H=0.10$ ) has a weak IRAC excess (§4.2). These stars are “debris disk candidates”. The star SO981 ( $J-H \sim 0.45$ ) shows no IRAC excess but has a modest  $24 \mu\text{m}$  excess, and thus is a likely debris disk system around a K early type star. However, a more detailed study of the debris disk candidates in this young stellar cluster is necessary to clarify the actual nature of their  $24 \mu\text{m}$  excesses, since contribution from primordial disk material could be present (Hernandez et al. 2006). There are 5 low mass star members ( $J-H > 0.5$ ) with weak IRAC excess, in which the excesses observed at the IRAC bands and at  $24 \mu\text{m}$  are consistent with a overall decrease of infrared emission from the inner and outer disks.

## 4.2. IRAC SED slope

Lada et al. (2006) showed the utility of characterizing excess infrared emission using the IRAC SED slope  $\alpha$  determined from the [3.6]-[8.0] color, where  $\alpha = d \log[\lambda F_\lambda] / d \log[\lambda]$ . In this system, IRAC class I candidates, defined as systems with  $\alpha > 0$ , are usually protostars; disk-bearing systems, having  $-2.56 \lesssim \alpha < 0$ , include IRAC class II stars and objects with weak IRAC excess (the lower limit depends upon spectral type and photometric errors, see below); and IRAC class III stars have essentially no inner disk emission, with  $\alpha < -2.56$  (again, depending upon spectral type and errors).

Figure 10 shows  $\alpha$  versus the [8.0] magnitude for members (filled symbols) and uncertain members (open symbols) of the cluster. Dashed lines represent the regions of differing levels of infrared excess as discussed above. We subdivide the disk-bearing stars into two categories: IRAC class II stars (squares,  $\alpha > -1.8$ ); and systems with less IRAC infrared excess, which Lada et al. (2006) termed “anemic” disks and which we call here “evolved disks” ( $-2.56 \lesssim \alpha < -1.8$ ).

Because the photometric uncertainties in  $\alpha$  increase with [8.0], a single straight line in Figure 10 to separate IRAC class III stars (in the IRAC wavelength range) and evolved disks is not useful. Lada et al. (2006) avoided this problem by applying their criteria to separate class III and evolved disks only to the brighter stars with spectral types M4.5 or earlier (the number of evolved disks would be overestimated in the lowest mass bins due to large photometric errors; C. Lada, private communication). We distinguish between IRAC class III stars (circles) and evolved disk systems (triangles) using the mean error of  $\alpha$  ( $\bar{\sigma}$ ) calculated from the photometric errors for stars within 0.5 magnitude bins. IRAC class III stars are those with excesses, if any, smaller than the  $3\bar{\sigma}$  deviation (solid lines) from the median  $\alpha$ .

We wish to examine the mass dependence of disk emission, but we do not have spectral types for most of these stars. As a proxy for mass, we use the J magnitude, which is relatively unaffected by disk excess emission, and convert to approximate mass ranges using the 3 Myr isochrone from Baraffe et al. (1998) for low mass ( $\leq 1 M_{\odot}$ ) stars and Siess et al. (2000) high mass ( $> 1 M_{\odot}$ ) stars, assuming a distance of 440 pc and  $E(B-V)=0.05$ . Figure 11 shows  $\alpha$  versus J, with the regions expected for objects in different ranges of mass: HAeBe range ( $> 2 M_{\odot}$ ), Intermediate Mass TTS (IMTTS) range (1.0-2.0  $M_{\odot}$ ), TTS range (0.1-1.0  $M_{\odot}$ ) and Brown dwarfs range ( $< 0.1 M_{\odot}$ ). Most of the objects with optically thick and evolved disks are located in the mass range of T Tauri stars.

Using the results from Figure 11, we derive the fractions of stars with optically-thick disks (filled circles + dotted line) and all disk-bearing stars (open circles + dashed line) versus J magnitude, with corresponding mass ranges indicated (see also Table 5). The lowest fraction of disks is observed in the highest mass stars (HAeBe range), in agreement with the fraction calculated for the overall population of OB1b sub-association (Hernández et al. 2005). There is a marginal evidence that the disk fraction declines toward lower masses (into the brown dwarf range), in agreement with results from Lada et al. (2006) for the young (2-3 Myr) stellar group IC 348. Nevertheless, including the error bars, the fraction is also consistent with no mass dependence toward lower masses. The fraction of thick disks in the TTS mass range agrees with the result from Oliveira et al. (2006,  $33 \pm 6\%$ ; ) for low mass stars.

Only  $15 \pm 5\%$  of disk-bearing stars in the TTS mass range are disk evolved objects, approximately in agreement with results from the 4 Myr-old cluster Tr 37 (10%; Sicilia-Aguilar et al. 2006), although with better statistics and higher photometric accuracy. If we assume a steady-state evolution of disks, and also assume that the evolved disks are going through a phase of clearing of small dust particles in the inner disk, then our observed frequency suggests a timescale of inner disk clearing  $\sim 0.15 \times 3 \text{ Myr} \sim 0.45 \text{ Myr}$ .

### 4.3. Disk diversity: SEDs

Figure 13 shows SEDs (data from IRAC, MIPS, 2MASS and optical B, V, R and I magnitudes when are available) for selected members. The first 5 rows show the SEDs of stars in the mass range of TTS ( $0.1-1.0 M_{\odot}$ ), while the last row shows the SEDs of stars in the mass range of HAeBe stars ( $>2 M_{\odot}$ ). SEDs (solid lines) are normalized to the J band and are sorted by different levels of IR excesses indicating differences in the disks. Each panel is labeled with the internal running identification number and the classification from the IRAC SED slope analysis (§4.2). The dotted line represents the median SED (Table 3) of optically thick disk stars in the mass range of TTS defined in Figure 11 (hereafter, optically thick disk median SED); error bars denote the quartiles of the distribution. This typical disk emission in the  $\sigma$  Orionis cluster is lower than the median in Taurus (D’Alessio et al. 1999, dot-dashed line in the first upper-left panel), which has an age of  $\sim 1-2$  Myr, indicating differences due to evolutionary effects such as grain growth and/or settling to the disk midplane (see also Sicilia-Aguilar et al. 2006; Lada et al. 2006), or lower accretion-rate (D’Alessio et al. 2006). The dashed lines represent the median photospheric SED (Table 4) in the T Tauri mass range.

The first row of Figure 13 shows the SEDs of evolved disk objects (SO905, SO1057, SO759 and SO587) which exhibit modest infrared disk emission. The lower level of infrared excess emission could be explained by decreasing the height of the irradiation surface in the disks due to a higher degree of settling, which diminishes the degree of flaring, thus producing flatter disk structures (D’Alessio et al. 2006). The second row of SEDs (SO120, SO1268, SO299 and SO897) shows some transition disk candidates, which exhibit little or no excess in IRAC bands but  $24 \mu\text{m}$  emission similar to optically thick disks. This indicates a removal of small dust particles in the inner disks but not depletion or removal in the outer disk. In the next rows, the stars SO818, SO1267, SO908, SO1156, SO540 and SO1266 show somewhat weaker IRAC excesses. The stars SO73, SO927, SO1154, SO1153, SO457, and SO668 show larger infrared excesses than the optically thick median, which might indicate more highly flared disk structure (D’Alessio et al. 2006; Dullemond & Dominik 2005), edge-on disks, or a contribution from an envelope. SO927 has strong emission in the  $H\alpha$  (Weaver & Babcock 2004). SO1153 (V510 Ori; HH 444) and SO1154 (HH 445) are Herbig-Haro objects producing collimated outflows (Andrews et al. 2004). Finally, SO457 has been identified by Oliveira & van Loon (2004) as a class I object.

In the last row of Figure 13, SEDs of earlier-type members are compared with photospheres of stars with similar spectral types (long dashed line Kenyon & Hartmann 1995). The star SO724 (B2; Guetter 1981) shows small excess at  $8 \mu\text{m}$  but has no excess at  $24 \mu\text{m}$ , this star was classified in §4.2 as an evolved disk object possibly due to a background PAH

contamination at  $8 \mu\text{m}$ . The stars SO913 (B9.5; Guetter 1981) and SO956 (A8; Guetter 1981) show small or no excesses in the IRAC bands but have significant excesses at  $24 \mu\text{m}$ , consistent with being debris disk stars. Finally, the star SO411, classified as class I candidate in §4.2, shows small excesses at wavelengths shorter than  $5.8 \mu\text{m}$  and a rising SED at longer wavelengths. This emission line star, with spectral type F5 (Gregorio-Hetem & Hetem 2002), could be an accreting transition disk object in the HAeBe mass range. This object alternatively could be considered to be an IMTTS, as F5 is the usual transition spectral type between HAeBe and IMTTS (see Hernández et al. 2004).

Most of the disk classifications using the IRAC SED slope (§4.2) agree with the results from analyzing SEDs. However, a few objects were reclassified taking into account the overall SEDs; these objects are labeled in Tables 1 and 2.

#### 4.4. Disk evolution

Figure 14 shows the fraction of stars in the TTS mass range with near-infrared disk emission in different stellar groups, as a function of age (Hernández et al. 2005; Haisch et al. 2001). Recent *Spitzer* results for the young stellar clusters NGC7129 (Gutermuth et al. 2004), Taurus (Hartmann et al. 2005c),  $\eta$  Chameleontis (Megeath et al. 2005a), Tr37 and NGC7160 (Sicilia-Aguilar et al. 2006), IC348 (Lada et al. 2006), and Upper Scorpius (Carpenter et al. 2006) have been included in this plot. The disk fractions shown in Figure 14 include stars with optically thick and evolved disks (disk-bearing stars) detected mostly using IRAC photometry. The  $\sigma$  Orionis cluster (filled square) follows (within the scatter of the distribution) the disk fraction trend outlined by in other stellar groups (Haisch et al. 2001; Hillenbrand et al. 2006).

Aside from the decrease in the disk fraction with age, the amount of infrared disk emission also decreases with age. Figure 15 shows the distribution of  $\alpha$  for low mass stars in the stellar groups Taurus (Hartmann et al. 2005c), IC348 (Lada et al. 2006),  $\sigma$  Orionis (this work) and Tr 37 (Sicilia-Aguilar et al. 2006). As in Figure 13, the youngest group, Taurus, has a larger population of stars with robust optically thick disks ( $\alpha > -1$ ). In contrast, in the more evolved stellar groups most disk-bearing stars have an  $\alpha < -1$ , indicating a reduction in the height of the disk photosphere (less disk flaring) in the inner regions.

The Taurus sample suggests a relatively clear break between stars without IRAC excesses and optically-thick disk systems (Hartmann et al. 2005c), although the sample size is relatively small. The  $\sigma$  Orionis sample also suggests a small fraction of objects with intermediate or evolved disk excesses, as discussed previously. The evolved disk fraction is less

certain in Tr 37, due to the larger photometric errors for that more distant cluster. The IC 348 sample suggests a larger fraction of evolved disks than seen in  $\sigma$  Ori; the reality of this possible difference requires further study.

In contrast to IC 348, the  $\sigma$  Orionis and Tr 37 clusters include high mass stars located in their center (O9 in  $\sigma$  Orionis cluster and O7 in Tr37); however, the medians of  $\alpha$  are similar in these stellar groups (Figure 15). This suggests that external photoevaporation in  $\sigma$  Orionis and Tr 37 may be not very important for disk dissipation.

#### 4.5. Spatial distribution of the $\sigma$ Orionis cluster

Figure 16 shows the spatial distribution of members with and without infrared excesses. As shown in the upper right panel, the space density has a peak with a FWHM of  $0.25^\circ$  (1.9 pc). The upper-left panel shows the ratio of systems with disks to the total members in radial distance bins defined by the semi-circles East-West versus the radial distance from the center of the cluster. Solid circles (+dotted line) represent the fraction of thick disks, while open circles (+dashed line) represent the total fraction of disk-bearing stars, defined in §4.3. The error bars represents the statistical  $N^{-1/2}$  error in our disk fractions, where N is the number of stars with disks. Similarly, the lower-right panel shows the fraction of disks in radial distance bins defined by the semi-circles North-South. In contrast to the result of Oliveira et al. (2006), using K and L band observations, there is evidence for a higher disk fraction near the cluster center. However, we cannot rule out a small, relatively uniform contamination of non-members which could also produce this effect.

There is a slight increase in the disk fraction in the north-east direction; in the direction toward NGC2024 (age  $< 1$  Myr,  $D \sim 440$  pc; Levine et al. 2006; Eisner & Carpenter 2003), located at  $\sim 1.0$  deg from the  $\sigma$  Orionis center; this fraction could be affected by disk-bearing members of this younger stellar group. Since NGC2024 is centrally concentrated, the fraction could be also affected by stars extends toward the Horsehead nebula (located at  $\sim 0.6$  deg from the  $\sigma$  Orionis center), which also shows several class II objects in separate *Spitzer* maps (Megeath et al. 2005b). Spectroscopic studies are necessary to test whether the disk fractions in the outer regions are affected by non-members.

#### 4.6. Disk and X-ray emission

A sub-sample of 81 stars have X-ray luminosities from Franciosini et al. (2006), including 8 evolved disks, 21 optically thick disks and 52 class III stars. Figure 17 shows the cumulative

distribution of class III stars and stars with optically thick disks as a function of X-ray luminosity. The significance level of 64% in a Kolmogorov-Smirnov (KS) test indicates that class III stars have similar X-ray luminosities as stars with disks. This suggests that the presence of optically thick disks have small or no influence on X-ray emission, such as might be caused by an accretion shock, in agreement with the results from Franciosini et al. (2006).

#### 4.7. Contamination expected in the uncertain members sample

Stars selected as uncertain members are relatively faint ( $J > 13.0$ ). From 133 stars in this sample, only 11 objects have IRAC SED slopes consistent with the presence of disks (10 thick disk + 1 evolved disks). So, the fraction of disk-bearing stars for the uncertain members ( $8.3 \pm 2.5$  %) is very low compared with the fraction of disk-bearing stars expected for members with  $J > 13$  in the  $\sigma$  Orionis cluster ( $31.3 \pm 4.8$ ). Assuming that the source of non-members are class III stars and the disk-bearing stars are actual members of the cluster, we can expect that at least 84 class III stars ( $\sim 70$  % of the uncertain member sample) do not belong to the  $\sigma$  Orionis cluster and are likely to be field M dwarfs or other sources of contaminations. Additional spectroscopic studies are essential to determine membership for this sample.

## 5. Conclusions

We have used the IRAC and MIPS instruments on board the *Spitzer* Space Telescope to study the frequencies and properties of disks around 336 members of the 3 Myr old  $\sigma$  Orionis cluster, with results for another 133 objects of uncertain membership. We confirm and strongly improve upon previous results showing that disk fractions are much lower around A-type and intermediate-mass T Tauri stars, implying that disk evolution is much more rapid for stars with masses  $> 1M_{\odot}$ . In particular, we find that only a few percent of all A-F stars have optically thick disks, with perhaps another  $\sim 15$  % having detectable optically-thin, probable debris disks. This fraction of probable debris disk is lower than those found in the older Orion OB1b (38%) and OB1a (46%) sub-associations, suggesting that  $\sigma$  Orionis cluster could be in a phase between the clearing of the primordial disk and the formation of large icy objects, which produce the second-generation dust observed in debris disk systems (Hernandez et al. 2006). The disk frequency  $\sim 30 - 35$ % we find for T Tauri stars is reasonably consistent with studies of other populations, perhaps a bit lower. We also find no evidence that the disk fraction decreases significantly among the highest-mass brown dwarfs. Overall, disk frequencies follows the overall trend of decreasing disk frequency with

increasing age observed in other young stellar populations.

About 15% of the T Tauri disk systems exhibit weak IRAC excesses inconsistent with simple optically-thick disk models. If these systems are in the process of clearing small dust particles from their inner disks, the observed fraction suggests that the timescale for this evolution is  $\lesssim 0.5$  Myr. We also find that the infrared excesses among optically-thick disks in  $\sigma$  Ori are systematically lower than the excesses observed from younger Taurus molecular cloud stars. This result confirms and strongly extends previous results indicating an overall decrease in the level of emission of optically-thick disks with age, which may indicate an overall settling of dust particles to the disk midplanes, or grain growth, or both. The populous nature and relatively near distance of the  $\sigma$  Orionis cluster allows us to improve the statistics of these correlations, providing an important step toward a full characterization of protoplanetary disk evolution in clustered environments, in which most stars form. Finally, we do not find correlation between X ray luminosity and the disk infrared excess, suggesting that the presence of optically thick disks have small or not influence on the X ray emission.

Thanks to R.D. Jeffries, D. Stern and C. Lada for insightful communications. This publication makes use of data products from the CIDA Equatorial Variability Survey, obtained with the J. Stock telescope at the Venezuela National Astronomical Observatory, which is operated by CIDA for the Ministerio de Ciencia y Tecnología of Venezuela, and Two Micron All Sky Survey, which is a joint project of the University of Massachusetts and the Infrared Processing and Analysis Center/California Institute of Technology. This work is based on observations made with the *Spitzer Space Telescope* (GO-1 0037 and GO-1 0058), which is operated by the Jet Propulsion Laboratory, California Institute of Technology under a contract with NASA. Support for this work was provided by University of Michigan and NASA Grant NAG5-13210.

### A. Previous membership studies

The  $\sigma$  Orionis cluster has been the subject of several photometric and spectroscopic studies to identify members of its population.. Analyzing the photometric and kinematic properties of the bright population in the cluster, Kharchenko et al. (2004) determined an angular size of 0.40 degrees and identified 7 stars with photometric and kinematic membership probabilities larger than 50%. Since the cluster is reasonably close, relatively young and has low reddening, many of the previous studies have focused on identifying low mass stars and substellar objects. Adopting an age interval of 2-7 Myr and the Hipparcos distance of the star  $\sigma$  Ori ( $352_{-85}^{+166}$  pc), Béjar et al. (1999, 2001, 2004) presented several lists

of low mass stars, brown dwarfs and free-floating planets belonging to the  $\sigma$  Orionis cluster, selected from optical and NIR color-magnitude diagrams. Adopting an age of 2.5 Myr and the distance calculated for OB1b subassociation (440 pc), Sherry et al. (2004) reported photometric membership for a sample of low mass stars (193 objects) based on the V versus V-I color-magnitude diagram. Sherry et al. (2004) found that the cluster has  $\sim 160$  members in the mass range from  $0.2 M_{\odot}$  to  $1.0 M_{\odot}$ . Adopting an age of 3 Myr and a distance of 350 pc, Scholz & Eislöffel (2004) reported photometric membership for 135 candidates of very low mass stars ( $<0.4 M_{\odot}$ ) using the color magnitude diagrams, I versus I-J, and photometric variability.

Zapatero Osorio et al. (2002) presented intermediate and low resolution spectra including the  $H\alpha$  and Li I  $\lambda 6708\text{\AA}$  lines and confirmed 25 low mass stars and 2 brown dwarfs as members of the cluster. Barrado y Navascués et al. (2003) confirmed 51 low mass stars and brown dwarfs as members using low resolution spectroscopic analysis of forbidden lines, as well as Li I  $\lambda 6708\text{\AA}$  and  $H\alpha$  lines. Kenyon et al. (2005) presented an intermediate-resolution spectroscopic study of 76 photometrically selected stars ranging in mass from  $0.04 M_{\odot}$  to  $0.3 M_{\odot}$ ; 57 stars were confirmed as members on the basis that they exhibit Li I  $\lambda 6708\text{\AA}$  in absorption, a weak Na I doublet ( $8183, 8195\text{\AA}$ ) indicating low surface gravity consistent with PMS status, and radial velocities expected for the kinematic properties of the cluster. Burningham et al. (2005) confirmed as members 38 low-mass stars using high-resolution spectroscopic analysis of Na I doublet. Kenyon et al. (2005) and Burningham et al. (2005) showed that optical photometric selection alone is very effective to identify low mass members belonging to the cluster, with small contamination by non-members for stars with  $I < 17$  magnitudes.

Recently, Oliveira et al. (2006) compiled 59 spectroscopic confirmed members of the cluster and studied the circumstellar disks of the sample using NIR data. Franciosini et al. (2006) detect 175 X-ray sources down to the substellar limit. Half of this sample could be new members of the cluster based on the X-ray emission as indicator of youth.

## REFERENCES

- Andre, P., Ward-Thompson, D., & Barsony, M. 2000, *Protostars and Planets IV*, 59
- Andrews, S. M., Reipurth, B., Bally, J., & Heathcote, S. R. 2004, *ApJ*, 606, 353
- Baltay, C., et al. 2002, *PASP*, 114, 780
- Baraffe, I., Chabrier, G., Allard, F., & Hauschildt, P. H. 1998, *A&A*, 337, 403

- Barrado y Navascués, D., Zapatero Osorio, M. R., Béjar, V. J. S., Rebolo, R., Martín, E. L., Mundt, R., & Bailer-Jones, C. A. L. 2001, *A&A*, 377, L9
- Barrado y Navascués, D., Béjar, V. J. S., Mundt, R., Martín, E. L., Rebolo, R., Zapatero Osorio, M. R., & Bailer-Jones, C. A. L. 2003, *A&A*, 404, 171
- Béjar, V. J. S., Zapatero Osorio, M. R. & Rebolo, R. 1999, *ApJ*, 521, 671
- Béjar, V. J. S., et al. 2001, *ApJ*, 556, 830
- Béjar, V. J. S., Zapatero Osorio, M. R., & Rebolo, R. 2004, *Astronomische Nachrichten*, 325, 705
- Bessell, M. S. & Brett, J. M. 1988, *PASP*, 100, 1134
- Briceño, C., Calvet, N., Hernández, J., Vivas, A. K., Hartmann, L., Downes, J. J., & Berlind, P. 2005, *AJ*, 129, 907.
- Briceño, C., Hartmann, L., Hernández, J., Calvet, N., Vivas, A. K., Furesz G., & Szentgyorgyi, A. 2006, submitted to *ApJ*.
- Brown, A. G., Walter, F. M., & Blaauw, A. 1998, in *ASP Conf. Ser.*, *The Orion Complex Revisited*, ed. M.J. McCaughrean & A. Burkert
- Brown, A. G. A., de Geus, E. J., & de Zeeuw, P. T. 1994, *A&A*, 289, 101
- Burningham, B., Naylor, T., Littlefair, S. P., & Jeffries, R. D. 2005, *MNRAS*, 356, 1583
- Caballero, J. A. 2005, *Astronomische Nachrichten*, 326, 1007
- Calvet, N., D’Alessio, P., Hartmann, L., Wilner, D., Walsh, A., & Sitko, M. 2002, *ApJ*, 568, 1008
- Calvet, N., Muzerolle, J., Briceño, C., Hernández, J., Hartmann, L., Saucedo, J. L., & Gordon, K. D. 2004, *AJ*, 128, 1294
- Calvet, N., et al. 2005, *ApJ*, 630, L185
- Carkner, L., Kozak, J. A., & Feigelson, E. D. 1998, *AJ*, 116, 1933
- Carpenter, J. M., Mamajek, E. E., Hillenbrand, L. A., & Meyer, M. R. 2006, *ArXiv Astrophysics e-prints*, arXiv:astro-ph/0609372
- Cohen, M., & Schwartz, R. D. 1976, *MNRAS*, 174, 137

- Cutri, R. M., et al. 2003, VizieR Online Data Catalog, 2246, 0.
- D’Alessio, P., Calvet, N., Hartmann, L., Lizano, S., & Cantó, J. 1999, ApJ, 527, 893
- D’Alessio, P., et al. 2005a, ApJ, 621, 461
- D’Alessio, P., Merín, B., Calvet, N., Hartmann, L., & Montesinos, B. 2005b, Revista Mexicana de Astronomía y Astrofísica, 41, 61.
- D’Alessio, P., Calvet, N., Hartmann, L., Franco-Hernández, R., & Servín, H. 2006, ApJ, 638, 314
- Dullemond, C. P. & Dominik, C. 2004, A&A, 417, 159
- Dullemond, C. P., & Dominik, C. 2005, A&A, 434, 971
- Eisner, J. A., & Carpenter, J. M. 2003, ApJ, 598, 1341
- Engelbracht, C. W., et al. 2006, in preparation.
- Fazio, G. G., et al. 2004, ApJS, 154, 39
- Franciosini, E., Pallavicini, R., & Sanz-Forcada, J. 2006, A&A, 446, 501
- Furlan, E., et al. 2006, ApJS, 165, 568
- Guetter, H. H. 1981, AJ, 86, 1057
- Gómez, M., & Kenyon, S. J. 2001, AJ, 121, 974
- Gordon, K. D., et al. 2005, PASP, 117, 503
- Gorlova, N., et al. 2004, ApJS, 154, 448
- Gregorio-Hetem, J., & Hetem, A. 2002, MNRAS, 336, 197
- Gutermuth, R. et al., 2006, in prep.
- Gutermuth, R. A., Megeath, S. T., Muzerolle, J., Allen, L. E., Pipher, J. L., Myers, P. C., & Fazio, G. G. 2004, ApJS, 154, 374
- Haisch, K. E., Lada, E. A., & Lada, C. J. 2001, ApJ, 553, L153
- Hartmann, L. 2005a, ASP Conf. Ser. 337: The Nature and Evolution of Disks Around Hot Stars, 337, 3

- Hartmann, L. 2005b, ASP Conf. Ser. 341: Chondrites and the Protoplanetary Disk, 341, 131
- Hartmann, L., Megeath, S. T., Allen, L., Luhman, K., Calvet, N., D’Alessio, P., Franco-Hernandez, R., & Fazio, G. 2005c, ApJ, 629, 881
- Herbst, W., & Shevchenko, V. S. 1999, AJ, 118, 1043
- Hernández, J., Calvet, N., Briceño, C., Hartmann, L., & Berlind, P. 2004, AJ, 127, 1682
- Hernández, J., Calvet, N., Hartmann, L., Briceño, C., Sicilia-Aguilar, A., & Berlind, P. 2005, AJ, 129, 856.
- Hernandez, J., Briceño, C., Calvet, N., Hartmann, L., Muzerolle, J., & Quintero, A. 2006, accepted in Astrophysical Journal.
- Hillenbrand, L., Carpenter, J., & Meyer, M., 2006, in preparation.
- Jeffries, R. D., Maxted, P. F. L., Oliveira, J. M., & Naylor, T. 2006, MNRAS, L62
- Kenyon, M. J., Jeffries, R. D., Naylor, T., Oliveira, J. M., & Maxted, P. F. L. 2005, MNRAS, 356, 89
- Kenyon, S. J. & Hartmann, L. 1995, ApJS, 101, 117
- Kenyon, S. J., & Hartmann, L. 1987, ApJ, 323, 714
- Kharchenko, N. V. 2001, Kinematika i Fizika Nebesnykh Tel, 17, 409.
- Kharchenko, N. V., Piskunov, A. E., Röser, S., Schilbach, E., & Scholz, R.-D. 2004, Astronomische Nachrichten, 325, 740.
- Lada, E. A., & Lada, C. J. 1995, AJ, 109, 1682
- Lada, C. J., et al. 2006, AJ, 131, 1574
- Landsman, W. B. 1993, ASP Conf. Ser. 52: Astronomical Data Analysis Software and Systems II, 52, 246
- Levine, J. L., Steinhauer, A., Elston, R. J., & Lada, E. A. 2006, ApJ, 646, 1215
- Lyra, W., Moitinho, A., van der Bliek, N. S., & Alves, J. 2006, A&A, 453, 101
- Megeath, S. T., Hartmann, L., Luhman, K. L., & Fazio, G. G. 2005a, ApJ, 634, L113

- Megeath, S. T., et al. 2005b, Massive star birth: A crossroads of Astrophysics, IAU Symposium Proceedings of the international Astronomical Union 227, Held 16-20 May, Italy, edited by Cesaroni, R.; Felli, M.; Churchwell, E.; Walmsley, M. Cambridge: Cambridge University Press, pp.383-388.
- Muzerolle, J., Hillenbrand, L., Calvet, N., Briceño, C., & Hartmann, L. 2003, ApJ, 592, 266
- Oliveira, J. M., Jeffries, R. D., van Loon, J. T., & Rushton, M. T. 2006, MNRAS, 369, 272
- Oliveira, J. M., & van Loon, J. T. 2004, A&A, 418, 663
- Oliveira, J. M., Jeffries, R. D., Kenyon, M. J., Thompson, S. A., & Naylor, T. 2002, A&A, 382, L22
- Preibisch, T., & Feigelson, E. D. 2005, ApJS, 160, 390
- Reach, W. et al. 2006, Infrared Array Camera Data Handbook, version 3.0, *Spitzer* Science Center, California Institute of Technology, Pasadena, California 91125 USA.
- Rieke, G. H., et al, 2004, ApJS, 154, 25
- Rieke, G. H., et al. 2005, ApJ, 620, 1010
- Scholz, A., & Eislöffel, J. 2004, A&A, 419, 249
- Sherry, W. H., Walter, F. M., & Wolk, S. J. 2004, AJ, 128, 2316
- Schlegel, D. J., Finkbeiner, D. P., & Davis, M. 1998, ApJ, 500, 525
- Sicilia-Aguilar, A., Hartmann, L. W., Hernández, J., Briceño, C., & Calvet, N. 2005, AJ, 130, 188
- Sicilia-Aguilar, A., et al. 2006, ApJ, 638, 897
- Siess, L., Dufour, E., & Forestini, M. 2000, A&A, 358, 593
- Stern, D., et al. 2005, ApJ, 631, 163
- Vivas, A. K., et al. 2004, AJ, 127, 1158
- Walter, F. M., Wolk, S. J., Freyberg, M., & Schmitt, J. H. M. M. 1997, Memorie della Societa Astronomica Italiana, 68, 1081
- Walter, F. M., Wolk, S. J., & Sherry, W. 1998, ASP Conf. Ser. 154: Cool Stars, Stellar Systems, and the Sun, 154, 1793

- Warren, W. H., Jr., & Hesser, J. E. 1978, *ApJS*, 36, 497
- Ward-Thompson, D., Hartmann, L., & Nutter, D. J. 2005, *MNRAS*, 357, 687
- Weaver, W. B., & Babcock, A. 2004, *PASP*, 116, 1035
- Weidenschilling, S. J. 1997, *Icarus*, 127, 290
- Wu, H., Cao, C., Hao, C.-N., Liu, F.-S., Wang, J.-L., Xia, X.-Y., Deng, Z.-G., & Young, C. K.-S. 2005, *ApJ*, 632, L79
- Zapatero Osorio, M. R., Béjar, V. J. S., Pavlenko, Y., Rebolo, R., Allende Prieto, C., Martín, E. L., & García López, R. J. 2002, *A&A*, 384, 937

Table 1. Members of the  $\sigma$  Orionis Cluster

SO ID	RA(2000) deg	DEC(2000) deg	[3.6] mag	[4.5] mag	[5.8] mag	[8.0] mag	[24.0] mag	V mag	Ref	Var	X-ray source	Disk type	Known member
9	84.32781	-2.67275	10.99 ± 0.03	10.97 ± 0.03	10.80 ± 0.03	10.92 ± 0.03	...	15.40 ± 0.05	q	0	...	III	9
27	84.34599	-2.54623	13.00 ± 0.03	12.94 ± 0.03	12.86 ± 0.04	12.99 ± 0.05	...	18.42 ± 0.02	9	...	...	III	...
41	84.35401	-2.86730	10.30 ± 0.03	10.31 ± 0.03	10.28 ± 0.03	10.25 ± 0.03	...	...	...	...	...	III	...
52	84.36209	-2.36497	10.54 ± 0.03	10.56 ± 0.03	10.50 ± 0.03	10.49 ± 0.03	...	13.77 ± 0.08	q	0	...	III	...
59	84.36683	-2.60175	12.65 ± 0.03	12.62 ± 0.03	12.51 ± 0.04	12.52 ± 0.04	...	17.64 ± 0.05	q	0	...	III	...
60	84.36792	-2.40508	12.87 ± 0.03	12.82 ± 0.03	12.82 ± 0.04	12.80 ± 0.05	...	18.08 ± 0.11	q	0	...	III	9
73	84.37888	-2.39521	10.90 ± 0.03	10.44 ± 0.03	10.04 ± 0.03	9.11 ± 0.03	5.64 ± 0.03	16.28 ± 0.10	q	1	...	II	9
74	84.37941	-2.52922	9.46 ± 0.03	9.39 ± 0.03	9.30 ± 0.03	9.32 ± 0.03	9.19 ± 0.04	...	...	...	...	III	...
77	84.38132	-2.40748	10.99 ± 0.03	10.98 ± 0.03	10.93 ± 0.03	10.93 ± 0.03	...	15.83 ± 0.11	q	1	...	III	9
82	84.38269	-2.75514	9.24 ± 0.03	9.21 ± 0.03	9.16 ± 0.03	9.20 ± 0.03	8.95 ± 0.04	9.42 ± 0.02	...	...	...	III	...
92	84.38811	-2.89332	10.59 ± 0.03	10.74 ± 0.03	10.64 ± 0.03	10.55 ± 0.03	...	14.99 ± 0.04	q	0	...	III	9
115	84.40181	-2.24377	10.74 ± 0.03	10.72 ± 0.03	10.67 ± 0.03	10.70 ± 0.03	...	15.49 ± 0.10	q	0	...	III	9
116	84.40192	-2.69906	14.19 ± 0.03	14.02 ± 0.03	13.98 ± 0.06	13.97 ± 0.09	...	...	...	...	...	III	1,2,3,6
117	84.40270	-2.56669	11.82 ± 0.03	11.83 ± 0.03	11.81 ± 0.03	11.76 ± 0.04	...	17.12 ± 0.05	q	0	...	III	9
123	84.40760	-2.76226	11.51 ± 0.03	11.47 ± 0.03	11.40 ± 0.03	11.44 ± 0.03	...	16.37 ± 0.05	q	1	...	III	9
124	84.40766	-2.83598	9.49 ± 0.03	9.54 ± 0.03	9.45 ± 0.03	9.44 ± 0.03	9.65 ± 0.05	...	...	...	...	III	...
147	84.42406	-2.48557	9.51 ± 0.03	9.50 ± 0.03	9.47 ± 0.03	9.53 ± 0.03	9.59 ± 0.04	10.90 ± 0.07	7	...	...	III	...
164	84.43706	-2.49920	9.91 ± 0.03	9.90 ± 0.03	9.91 ± 0.03	9.89 ± 0.03	9.80 ± 0.05	10.95 ± 0.09	7	...	...	III	...
165	84.43856	-2.48111	12.65 ± 0.03	12.58 ± 0.03	12.55 ± 0.04	12.49 ± 0.04	...	18.76 ± 0.13	9	...	...	III	9
168	84.43889	-2.73678	8.96 ± 0.03	9.02 ± 0.03	8.95 ± 0.03	8.95 ± 0.03	8.94 ± 0.04	10.66 ± 0.07	7	...	...	III	...
194	84.45671	-2.60506	10.12 ± 0.03	10.17 ± 0.03	10.06 ± 0.03	10.10 ± 0.03	10.03 ± 0.06	...	...	...	...	III	...
209	84.46288	-2.43542	13.64 ± 0.03	13.53 ± 0.03	13.68 ± 0.05	13.38 ± 0.07	...	...	...	...	...	III	2,3
214	84.46497	-2.59045	10.81 ± 0.03	10.80 ± 0.03	10.79 ± 0.03	10.72 ± 0.03	...	15.64 ± 0.01	9	...	1	III	8,9
219	84.46685	-2.60126	13.92 ± 0.03	13.81 ± 0.03	13.73 ± 0.05	13.70 ± 0.07	...	...	...	...	0	III	6
220	84.46747	-2.56052	11.85 ± 0.03	11.85 ± 0.03	11.78 ± 0.03	11.77 ± 0.04	...	16.89 ± 0.03	9	...	0	III	9,12
229	84.47091	-2.55951	9.45 ± 0.03	9.46 ± 0.03	9.43 ± 0.03	9.42 ± 0.03	9.40 ± 0.04	...	...	...	1	III	...
240	84.47515	-2.74462	11.92 ± 0.03	11.88 ± 0.03	11.86 ± 0.03	11.82 ± 0.03	...	17.02 ± 0.05	q	0	...	III	8,9
243	84.47665	-2.65823	8.51 ± 0.03	8.68 ± 0.03	8.55 ± 0.03	8.51 ± 0.03	8.47 ± 0.03	10.91 ± 0.07	7	...	1	III	7
244	84.47683	-2.72711	8.99 ± 0.03	9.06 ± 0.03	8.98 ± 0.03	8.96 ± 0.03	8.98 ± 0.04	...	...	...	...	III	...
247	84.47852	-2.68587	12.04 ± 0.03	11.80 ± 0.03	11.45 ± 0.03	10.82 ± 0.03	8.41 ± 0.03	18.55 ± 0.06	q	0	0	II	5,9
251	84.47960	-2.46006	12.45 ± 0.03	12.36 ± 0.03	12.30 ± 0.04	12.46 ± 0.04	...	18.49 ± 0.10	9	...	...	III	9
254	84.48156	-2.55146	13.66 ± 0.03	13.35 ± 0.03	12.94 ± 0.04	12.32 ± 0.04	9.70 ± 0.05	...	...	...	0	II	2,3,12
256	84.48218	-2.40933	13.79 ± 0.03	13.74 ± 0.03	13.56 ± 0.06	13.77 ± 0.10	...	...	...	...	...	III	2,3
260	84.48530	-2.73263	11.91 ± 0.03	11.96 ± 0.03	11.85 ± 0.03	11.86 ± 0.03	...	16.84 ± 0.05	q	0	...	III	9
271	84.48935	-2.64562	12.92 ± 0.03	12.76 ± 0.03	12.58 ± 0.04	12.03 ± 0.04	9.40 ± 0.04	...	...	...	0	II	1,2,3,6,8,12
275	84.49076	-2.91668	11.62 ± 0.03	11.62 ± 0.03	11.60 ± 0.03	11.55 ± 0.03	...	14.86 ± 0.04	q	1	...	III	...
283	84.49328	-2.69059	12.06 ± 0.03	11.96 ± 0.03	11.90 ± 0.03	11.96 ± 0.04	...	18.92 ± 0.07	q	0	0	III	6,9,12
293	84.49872	-2.85090	9.61 ± 0.03	9.70 ± 0.03	9.62 ± 0.03	9.59 ± 0.03	9.67 ± 0.04	...	...	...	...	III	...
297	84.50228	-2.75267	11.56 ± 0.03	11.47 ± 0.03	11.47 ± 0.03	11.43 ± 0.03	...	17.75 ± 0.06	q	0	1	III	9,12
299	84.50394	-2.43548	11.68 ± 0.03	11.76 ± 0.03	11.66 ± 0.03	11.33 ± 0.03	6.76 ± 0.03	16.70 ± 0.11	q	1	...	TD <sup>2</sup>	9
300	84.50434	-2.76042	10.12 ± 0.03	9.70 ± 0.03	9.29 ± 0.03	8.64 ± 0.03	5.87 ± 0.03	17.59 ± 0.07	q	1	...	II	9

Note. — Table 1 is published in its entirety in the electronic edition of the *Astrophysical Journal*. A portion is shown here for guidance regarding its form and content.

References in columns 10 and 14: q CIDA survey; 1 Barrado y Navascués et al. (2003); 2 Béjar et al. (1999); 3 Béjar et al. (2001); 4 Béjar et al. (2004); 5 Burningham et al. (2005); 6 Kenyon et al. (2005); 7 Kharchenko et al. (2004); 8 Oliveira et al. (2006); 9 Sherry et al. (2004); 10 Scholz & Eislöffel (2004); 11 Zapatero Osorio et al. (2002); 12 Jeffries et al. (2006)

Column 11: 1 variable; 0 non-variable

Column 12: 1 X-ray emission; 0 not X-ray emission

Column 13: III=non-excess, II=thick disk, I=class I candidate, EV= evolved disk, TD=transition disk candidate, DD=Debris disk candidate

<sup>1</sup>Classified as III in §4.2

<sup>2</sup>Classified as EV in §4.2

<sup>3</sup>Classified as II in §4.2

<sup>4</sup>Classified as I in §4.2

Table 2. Uncertain members of the  $\sigma$  Orionis Cluster

SO ID	RA(2000) deg	DEC(2000) deg	[3.6] mag	[4.5] mag	[5.8] mag	[8.0] mag	[24.0] mag	Disk type
33	84.34808	-2.74109	14.49 ± 0.03	14.46 ± 0.04	14.42 ± 0.07	14.44 ± 0.15	...	III
47	84.35836	-2.34652	13.53 ± 0.03	13.55 ± 0.03	13.47 ± 0.05	13.80 ± 0.11	...	III
57	84.36604	-2.51190	13.45 ± 0.03	13.45 ± 0.03	13.33 ± 0.04	13.52 ± 0.08	...	III
71	84.37812	-2.40533	14.45 ± 0.03	14.48 ± 0.04	14.51 ± 0.11	14.21 ± 0.13	...	III
81	84.38234	-2.40128	14.36 ± 0.03	14.27 ± 0.04	14.19 ± 0.07	14.13 ± 0.14	...	III
87	84.38534	-2.75422	13.67 ± 0.03	13.70 ± 0.04	13.86 ± 0.08	13.96 ± 0.15	...	III
107	84.39636	-2.44933	12.10 ± 0.03	12.01 ± 0.03	11.91 ± 0.03	11.94 ± 0.03	...	III
120	84.40674	-2.42888	13.48 ± 0.03	13.49 ± 0.03	13.35 ± 0.05	13.30 ± 0.09	9.95 ± 0.05	TD <sup>1</sup>
219	84.46685	-2.60126	13.92 ± 0.03	13.81 ± 0.03	13.73 ± 0.05	13.70 ± 0.07	...	III <sup>6</sup>
127	84.40806	-2.80576	12.78 ± 0.03	12.82 ± 0.03	12.80 ± 0.04	12.73 ± 0.04	...	III
134	84.41515	-2.30742	14.14 ± 0.03	13.93 ± 0.03	13.87 ± 0.06	13.74 ± 0.08	...	III
154	84.43077	-2.44282	14.48 ± 0.03	14.45 ± 0.04	14.35 ± 0.08	14.15 ± 0.09	...	III
174	84.44174	-2.45832	13.71 ± 0.03	13.63 ± 0.03	13.61 ± 0.05	13.53 ± 0.08	...	III
188	84.45503	-2.36186	14.14 ± 0.03	14.17 ± 0.04	13.94 ± 0.06	14.06 ± 0.13	...	III
207	84.46257	-2.32070	14.13 ± 0.03	14.18 ± 0.03	14.14 ± 0.07	14.20 ± 0.11	...	III
221	84.46809	-2.44730	14.24 ± 0.03	14.22 ± 0.03	14.29 ± 0.07	14.10 ± 0.12	...	III
236	84.47451	-2.48824	14.48 ± 0.03	14.46 ± 0.04	14.07 ± 0.07	14.13 ± 0.13	...	III

Note. — Table 2 is published in its entirety in the electronic edition of the *Astrophysical Journal*. A portion is shown here for guidance regarding its form and content.

Column 9: III=non-excess, II=thick disk, I=class I candidate, EV= evolved disk, TD=transition disk candidate, DD=Debris disk candidate

<sup>1</sup>Classified as III in §4.2

<sup>2</sup>Classified as EV in §4.2

<sup>3</sup>Classified as II in §4.2

<sup>4</sup>Classified as I in §4.2

<sup>5</sup>Possible giant in the J-H versus H-K color-color diagram

<sup>6</sup>Radial velocity consistent for stars in the older population (Jeffries et al. 2006)

Table 3. Median SEDs and Quartiles of optically thick disk stars

Wavelength $\mu\text{m}$	Median $\log \frac{\lambda F_\lambda}{1.24 F_J}$	Upper	Lower	stars used
0.44	-1.506	-1.254	-1.654	22
0.55	-1.002	-0.842	-1.274	51
0.64	-0.738	-0.588	-0.928	60
0.79	-0.308	-0.220	-0.376	52
1.24	0.0	0.0	0.0	64
1.66	-0.037	-0.005	-0.065	64
2.16	-0.209	-0.125	-0.245	64
3.6	-0.563	-0.400	-0.645	64
4.5	-0.733	-0.580	-0.836	64
5.8	-0.910	-0.748	-0.978	64
8.0	-0.962	-0.804	-1.076	64
24	-1.238	-1.029	-1.430	58

Table 4. Median SEDs and Quartiles of non-excess stars

Wavelength $\mu\text{m}$	Median $\log \frac{\lambda F_\lambda}{1.24 F_J}$	Upper	Lower	stars used
0.44	-1.360	-1.206	-1.550	60
0.55	-0.863	-0.610	-1.166	116
0.64	-0.597	-0.400	-0.870	128
0.79	-0.204	-0.144	-0.324	97
1.235	0	0	0	137
1.662	-0.057	-0.037	-0.073	137
2.159	-0.257	-0.241	-0.273	137
3.6	-0.748	-0.733	-0.777	137
4.5	-1.038	-1.007	-1.083	137
5.8	-1.306	-1.278	-1.348	137
8.0	-1.693	-1.660	-1.723	137
24	-3.259	-3.198	-3.431	42 <sup>1</sup>

<sup>1</sup>Including stars in the mass range of IMTTS and HAeBe

Table 5. Disk fractions in the  $\sigma$  Orionis cluster

Range	Thick Disks %	Thick+Evolved Disks %
HAeBe	3.7±3.7	14.8±7.4
IMTTS	19.6±5.9	26.8±6.9
TTS	31.1±3.8	36.3±4.1
BDwarfs	29.7±9.0	33.3±9.7
Total	26.6±2.8	33.9±3.1

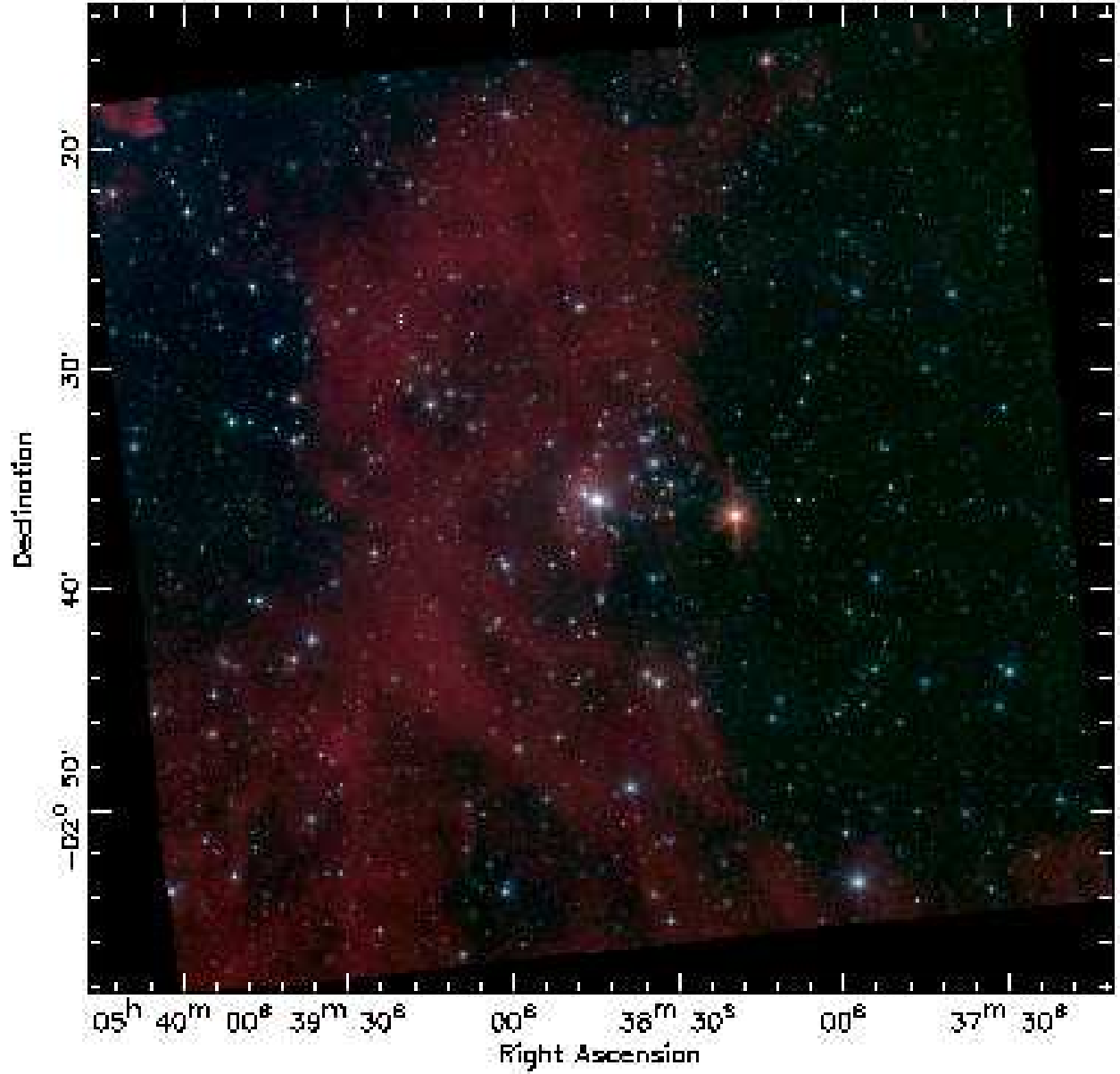


Fig. 1.— False-color image of the  $\sigma$  Orionis cluster. It is a 3-color composite of IRAC images, 3.6 (blue), 4.5 (green), and 8.0 (red)  $\mu\text{m}$ . The field is centering at the star  $\sigma$  Ori.

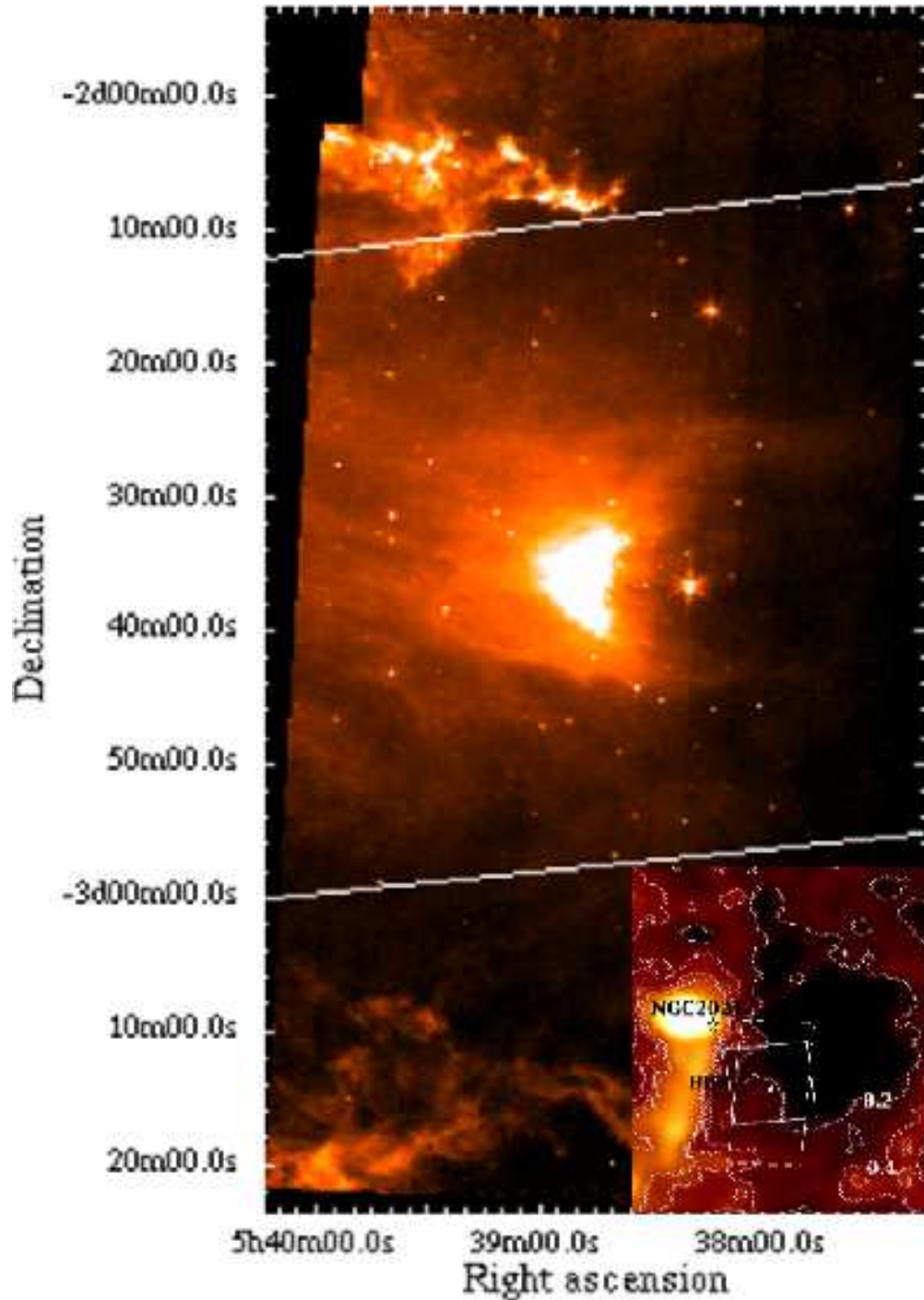


Fig. 2.— MIPS 24  $\mu\text{m}$  image of the  $\sigma$  Orionis cluster. The solid diagonal lines indicate the IRAC field. The lower-right panel shows a map of dust infrared emission (Schlegel et al. 1998) illustrating the location of the cluster in the OB1b sub-association (ring-like structure; Briceño et al. 2005); the isocontours indicate levels of galactic extinction ( $A_V=0.2, 0.4, 0.6$  &  $0.8$  mag). The IRAC (small box) and MIPS (large box) fields are shown in the inset. The positions of the young stellar cluster ( $<1$  Myr) NGC 2024 and the Horsehead nebula are also indicated in this figure

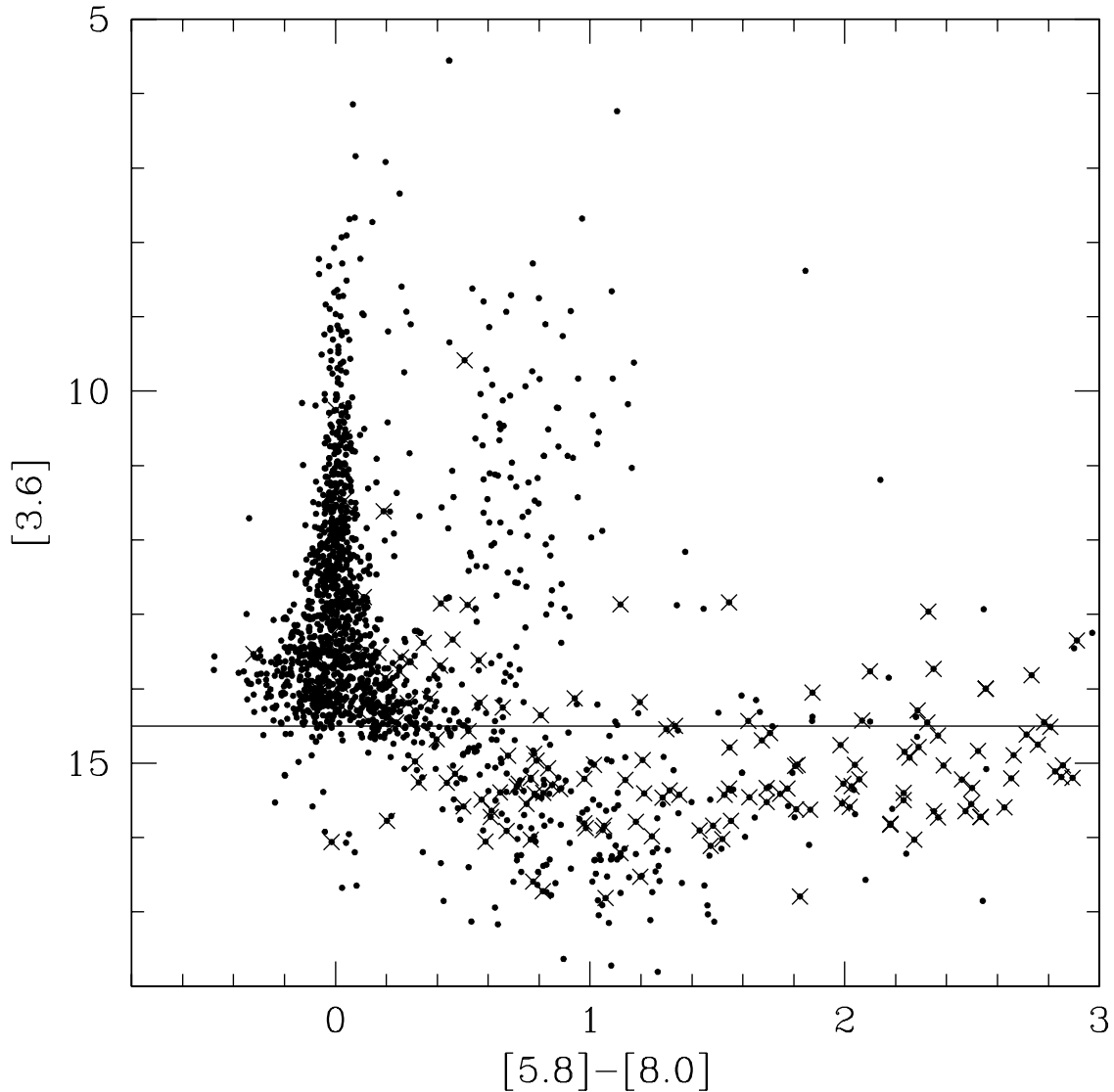


Fig. 3.—  $[5.8]-[8.0]$  versus  $[3.6]$  color-magnitude diagram. Objects with large FWHM in the radial profile measured in all IRAC bands are likely to be extended sources (crosses). The density of objects with photospheric colors ( $[5.8]-[8.0] \sim 0$ ) decreases drastically for sources with  $[3.6] > 14.5$ , most objects below this limit (solid line) are extended sources. We selected objects above the solid line, where the contamination from extragalactic sources is expected to be less than 50% (Fazio et al. 2004).

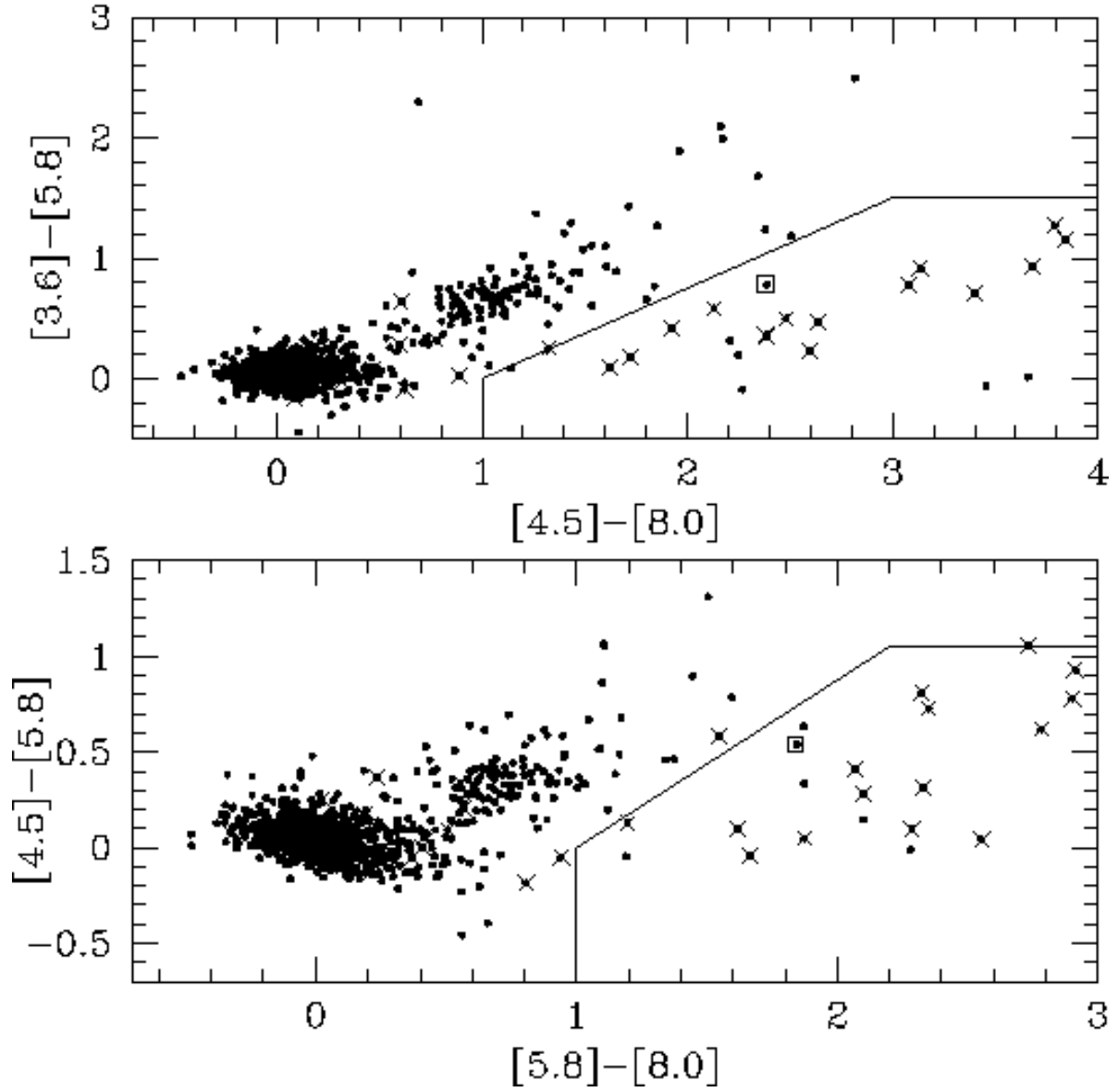


Fig. 4.— IRAC color-color diagrams illustrating the color selection used to reject PAH-rich galaxies. Symbols are the same as in Figure 3. Objects located redward from the solid lines are likely to be galaxies or faint companions with photometry affected by the primary stars of the stellar system. The open square is the star HD294268 (SO411)

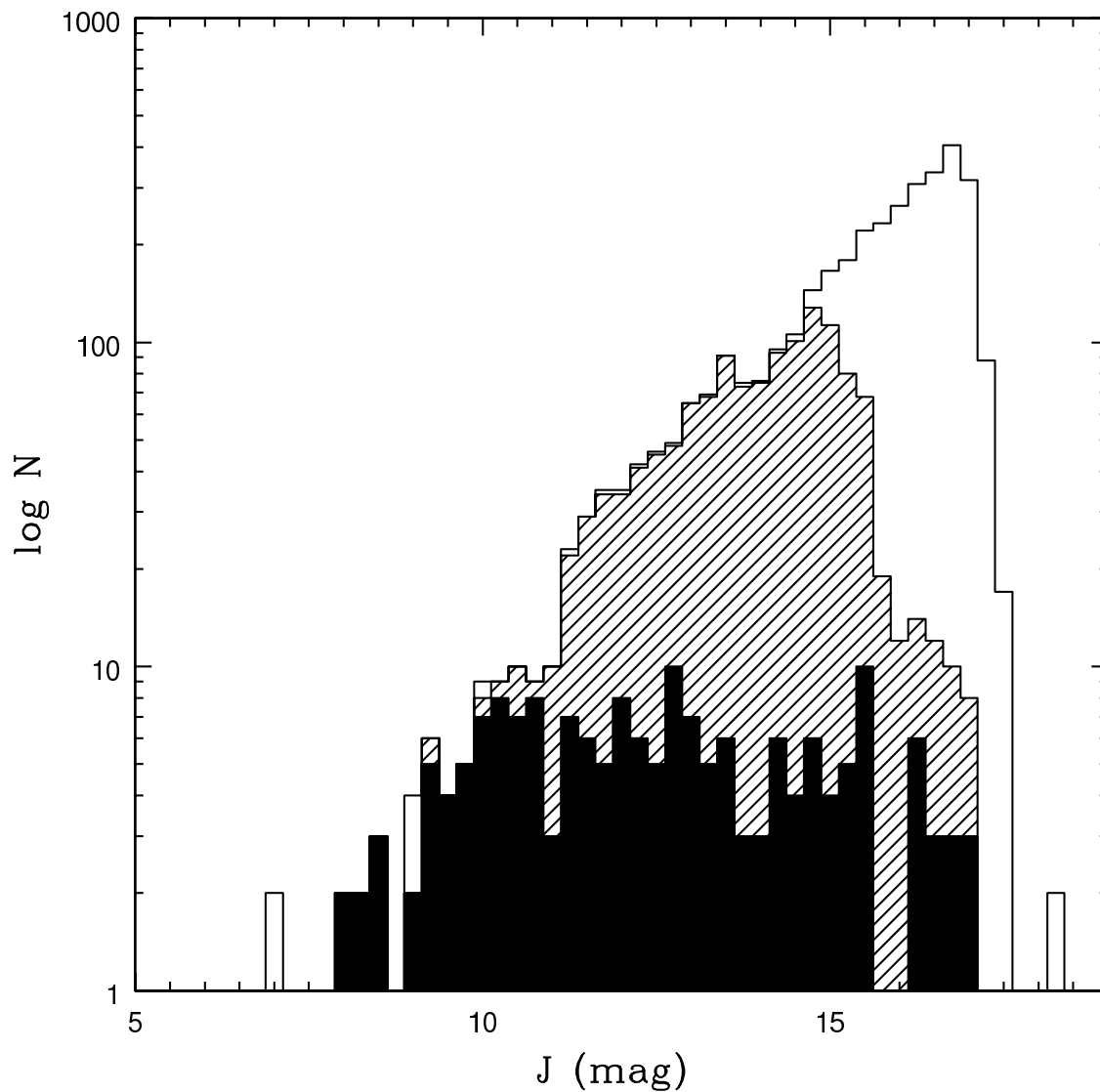


Fig. 5.— 2MASS J magnitude distribution: the open histogram represents all the 2MASS sources located in the IRAC field. Striped and solid histograms represent the 2MASS sources detected in IRAC and MIPS, respectively. Our completeness limit for sources with  $[3.6] < 14.5$  (see Figure 3) is  $J \sim 14$ . Most objects with  $J < 11$  have MIPS detections.

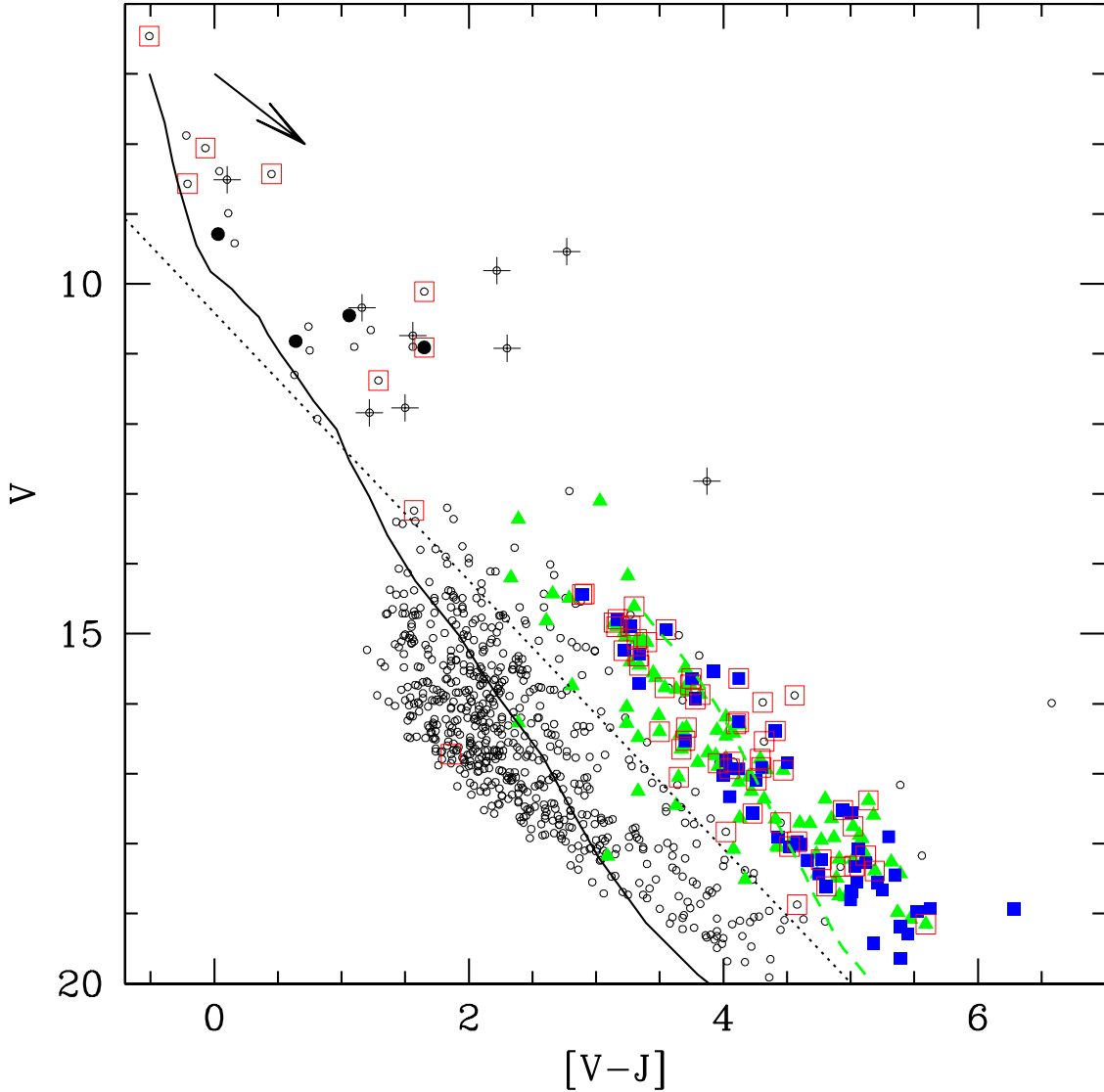


Fig. 6.—  $V$  versus  $V-J$  color-magnitude diagram, illustrating the selection of members of the  $\sigma$  Orionis cluster. Open circles represent stars in *Sample 2*. Solid symbols represent previous known members: photometric members (filled triangles), spectroscopic members (filled squares), and members selected by Kharchenko et al. (2004) combining photometric and astrometric data (filled circles). Stars with low membership probability combining photometric and astrometric data are labeled with the plus symbol. Open squares represent the X-ray sources in the sample (Franciosini et al. 2006). The ZAMS from (Siess et al. 2000) is represented as solid line and the 3 Myr isochrone from Baraffe et al. (1998) is represented as a dashed line. The arrow represents the reddening vector ( $A_V=1$ ). The membership limit is defined by the dotted line; stars located blueward from this limit are rejected as likely non-members of the  $\sigma$  Orionis cluster [See electronic edition of the journal for a color version of this Figure]

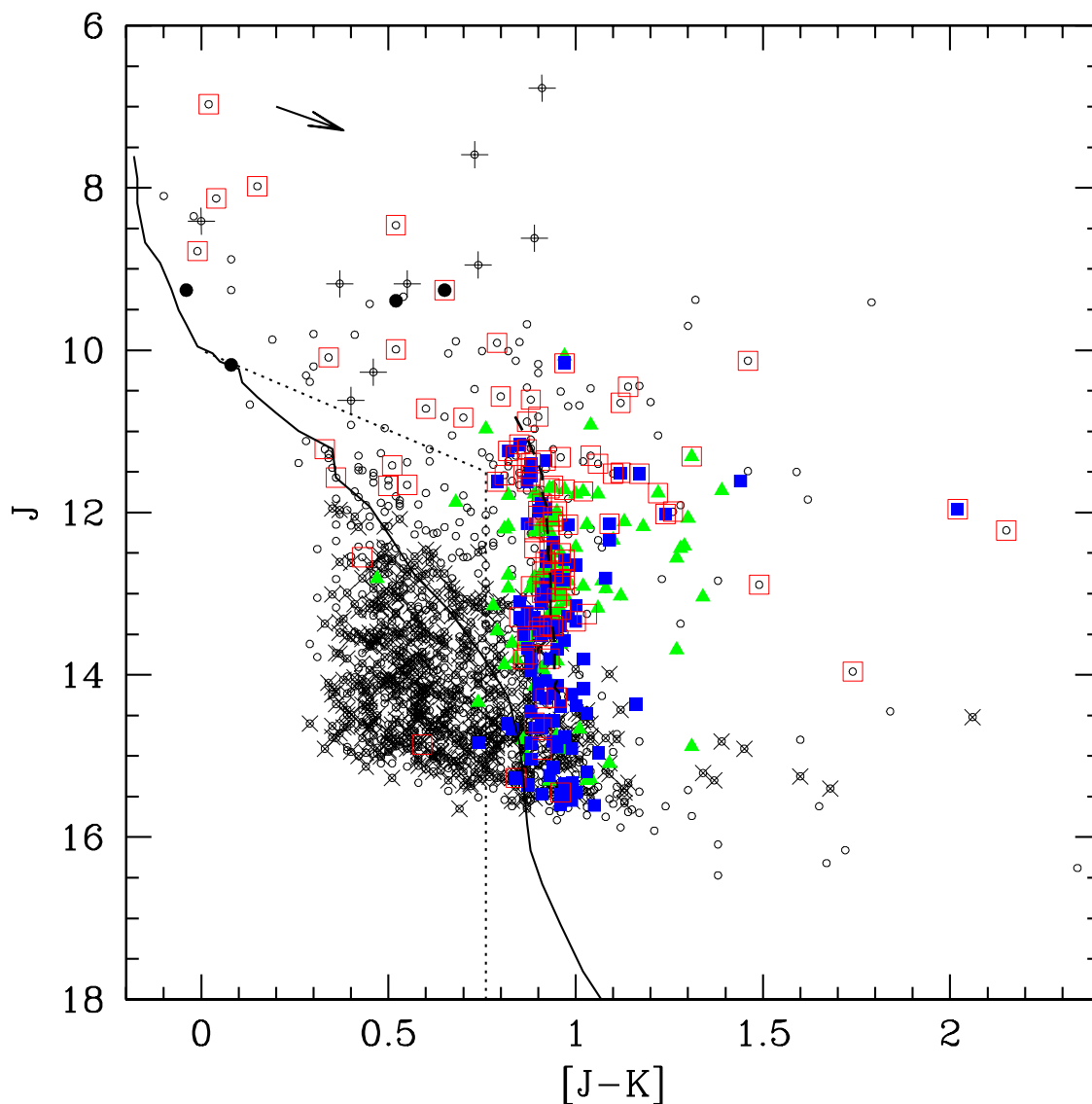


Fig. 7.— J versus J-K color-magnitude diagram, illustrating the selection of members of the  $\sigma$  Orionis cluster. Symbols are similar to Figure 6. Stars rejected as likely non-members in Figure 6 are represented with crosses. The arrow represents the reddening vector ( $A_V=1$ ). Contamination by non-members are expected for stars with  $J>13$ . We reject as non-members of the  $\sigma$  Orionis cluster stars located blueward from the dotted line. Stars selected using only the criterion defined in this plot are cataloged as uncertain members [See electronic edition of the journal for a color version of this Figure]

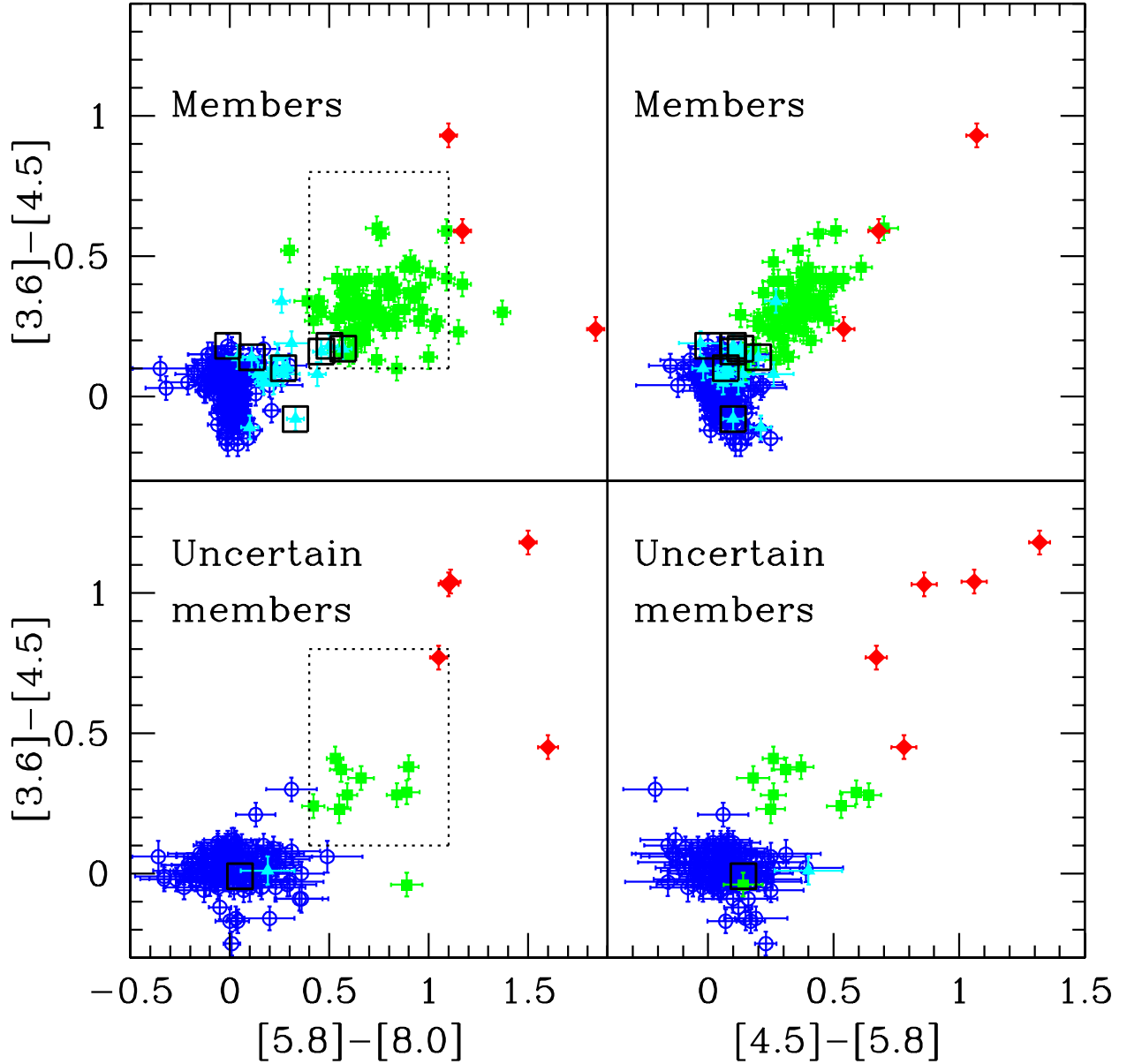


Fig. 8.— IRAC color color diagrams,  $[5.8]-[8.0]$  versus  $[3.6]-[4.5]$  (left panels) and  $[5.8]-[8.0]$  versus  $[4.5]-[5.8]$  (right panels). Members are plotted in the upper panels and uncertain members are plotted in the lower panels. Dashed box represents the loci of CTTS with different accretion rates (D’Alessio et al. 2005b). Open circles, filled triangles, filled squares and filled diamonds represent IRAC class III stars, stars with weak IRAC excess, IRAC class II stars and IRAC class I candidate (classified in §4.2), respectively. Objects surrounded by open squares are transition disk candidates (see Figure 9) [See electronic edition of the journal for a color version of this Figure]

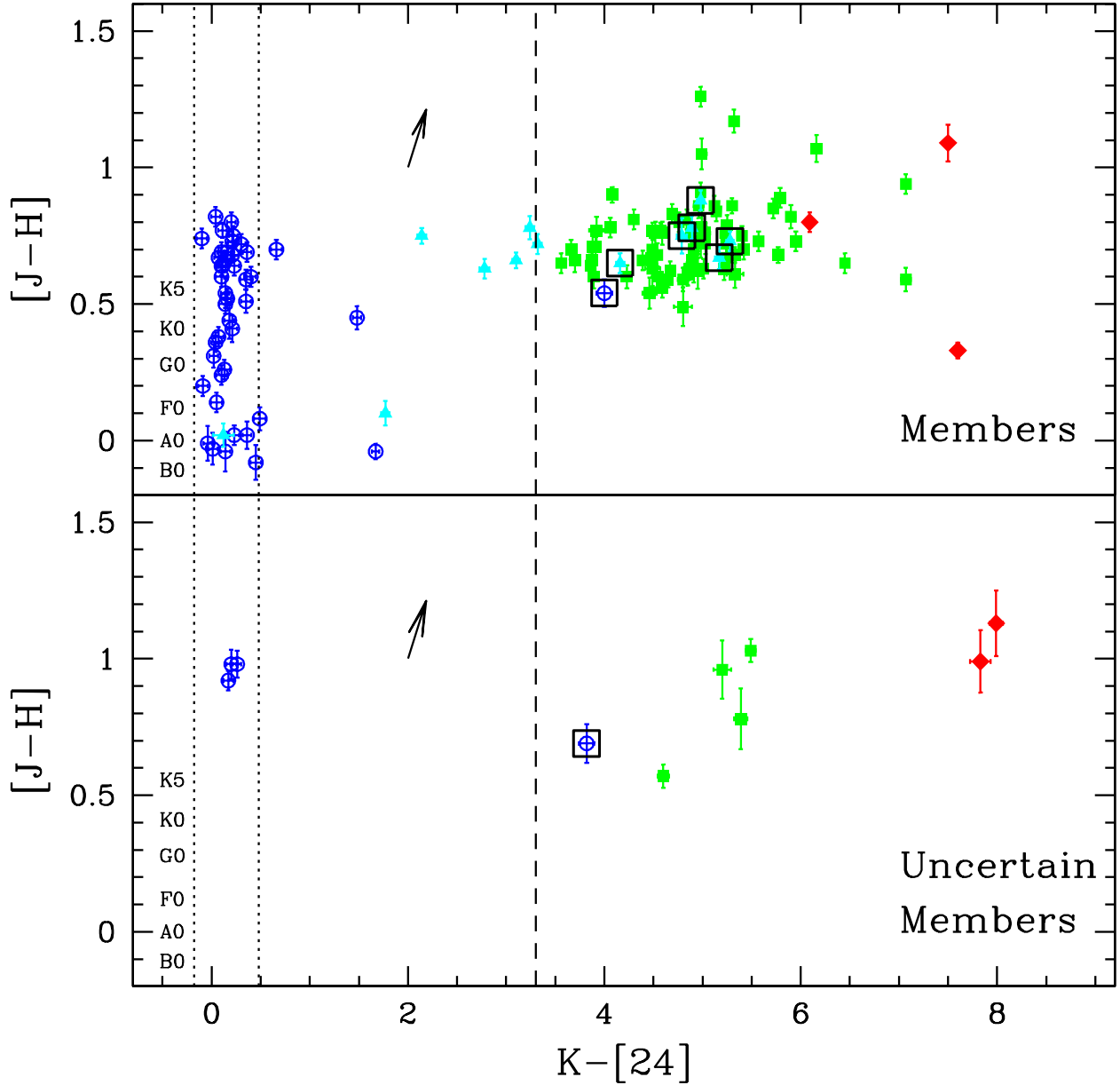


Fig. 9.—  $[J-H]$  versus  $K-[24]$  color-magnitude diagrams for members (upper panel) and uncertain members (lower panel) in the  $\sigma$  Orionis cluster. Symbols are similar to Figure 8. Dotted lines define the locus expected for non emission stars. The dashed line at  $K-[24]=3.3$  (the color of the debris disk star  $\beta$  Pic) indicates the limit between optically thick disk objects and evolved disk objects; transition disk candidates are stars classified as IRAC class III or evolved disk objects located redward from the dashed line (objects surrounded by open squares). In general, the IRAC class I candidates are locate redward from the optically thick disk objects. The arrow represents the reddening vector ( $A_V=2$ ) [See electronic edition of the journal for a color version of this Figure]

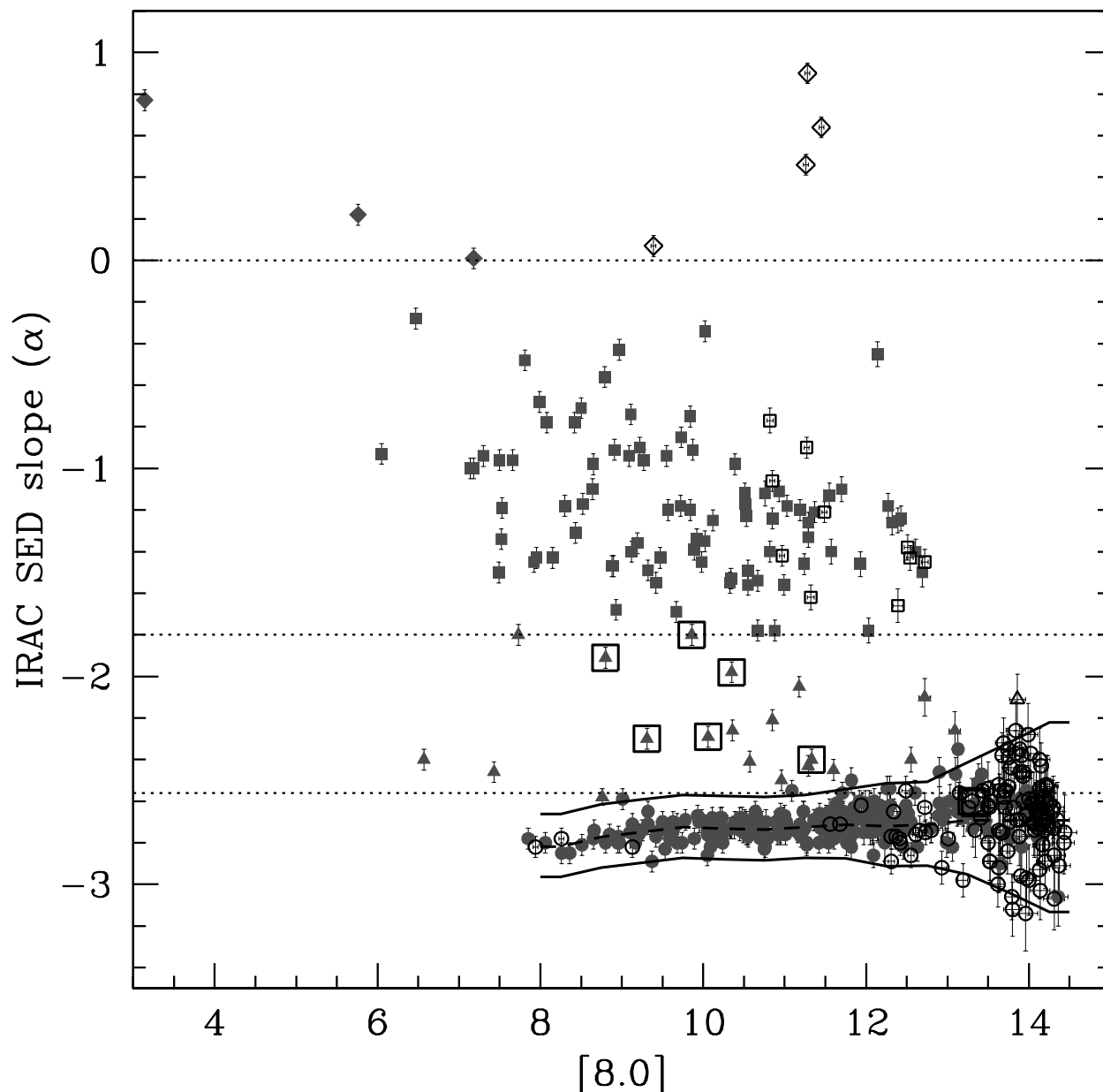


Fig. 10.— IRAC SED slope versus [8.0] for members (filled symbols) and uncertain members (open symbols) in the  $\sigma$  Orionis cluster. Dotted lines represent the limits from Lada et al. (2006) for different objects: IRAC class III stars (circles), IRAC class II stars (squares) and evolved disk objects (triangles). The dashed line represents the  $\alpha$  median for IRAC class III stars. The solid lines represent  $3\sigma$  values around this median; we adopt the solid upper line as the boundary between IRAC class III stars and evolved disk stars. The dotted line at  $\alpha=0$  indicates the boundary between IRAC class II stars and objects with flat or rising SED, class I candidates (diamonds). Class III stars and evolved disk objects surrounded by open squares are transition disk candidates, since they show strong  $24\ \mu\text{m}$  excess consistent with having an optically thick disk [See electronic edition of the journal for a color version of this Figure]

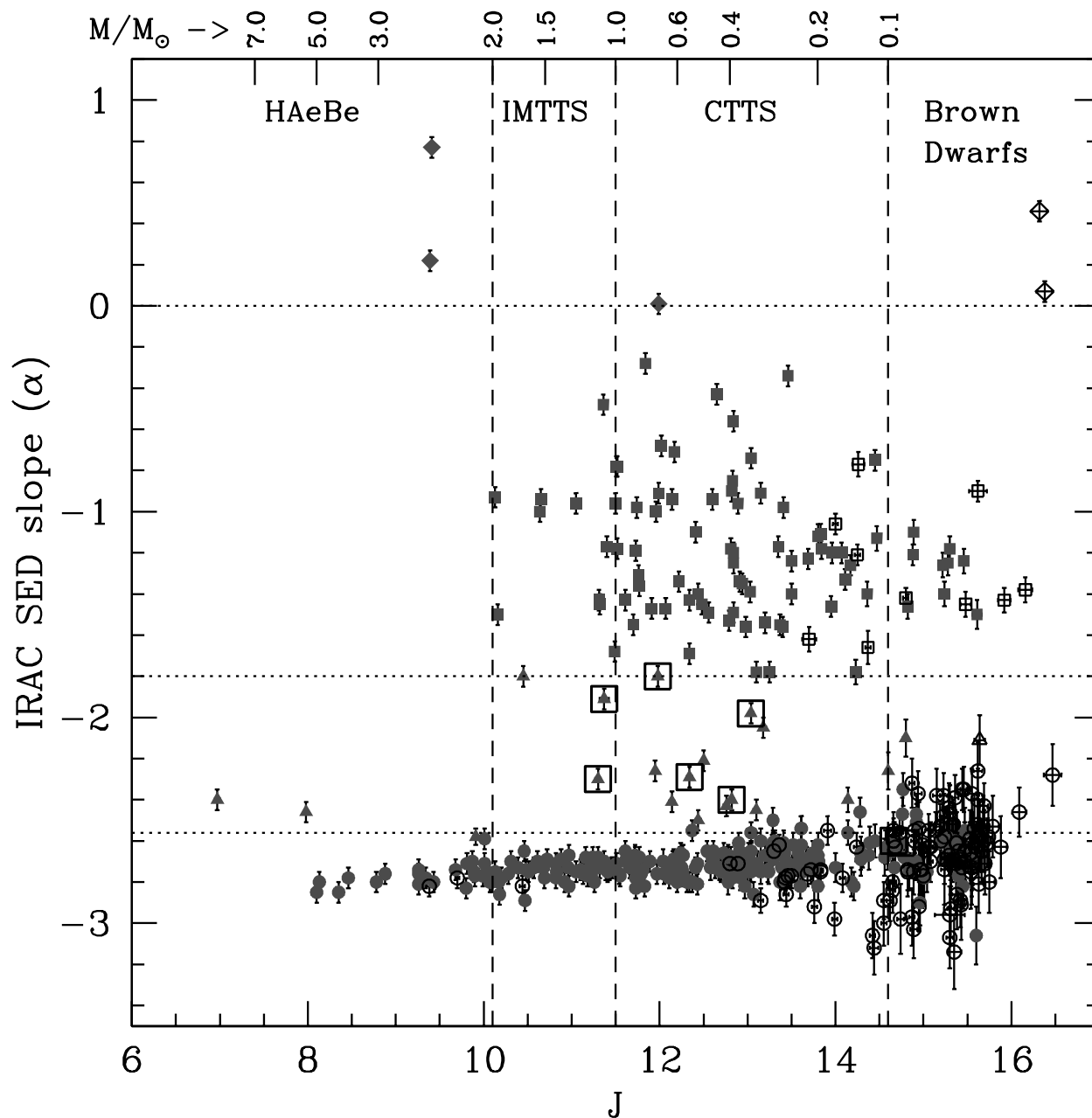


Fig. 11.— IRAC SED slope versus J magnitude for stars in the  $\sigma$  Orionis cluster. Symbols are as in Figure 10. Vertical dashed lines indicate approximate mass ranges defined using 3 Myr evolutionary models from Baraffe et al. (1998, for  $<1 M_{\odot}$ ) and from Siess et al. (2000, for  $>1 M_{\odot}$ ), assuming a distance of 440 pc and a reddening of  $E(B-V)=0.05$  [See electronic edition of the journal for a color version of this Figure]

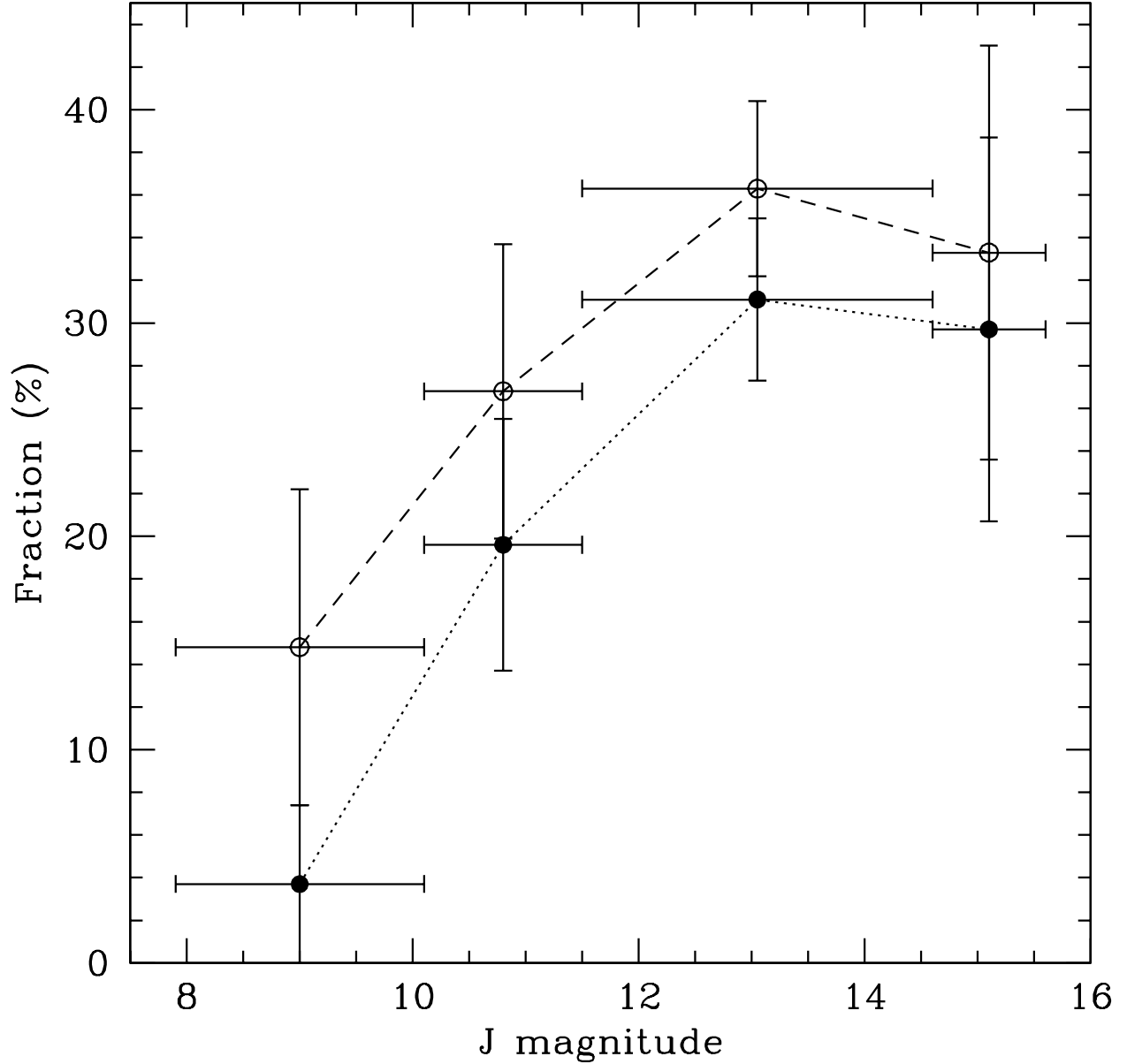


Fig. 12.— Disk fraction versus J magnitude. Each point represents a different mass range (see Figure 11): from left-to-right, HAeBe, IMTTS, TTS and Brown Dwarfs. Solid circles + dotted line indicate thick disks fraction. Open circles + dashed line are the fraction of disk-bearing stars. The lowest disk fraction is observed in the HAeBe mass range, while the highest frequency of disks is observed in the TTS mass range.

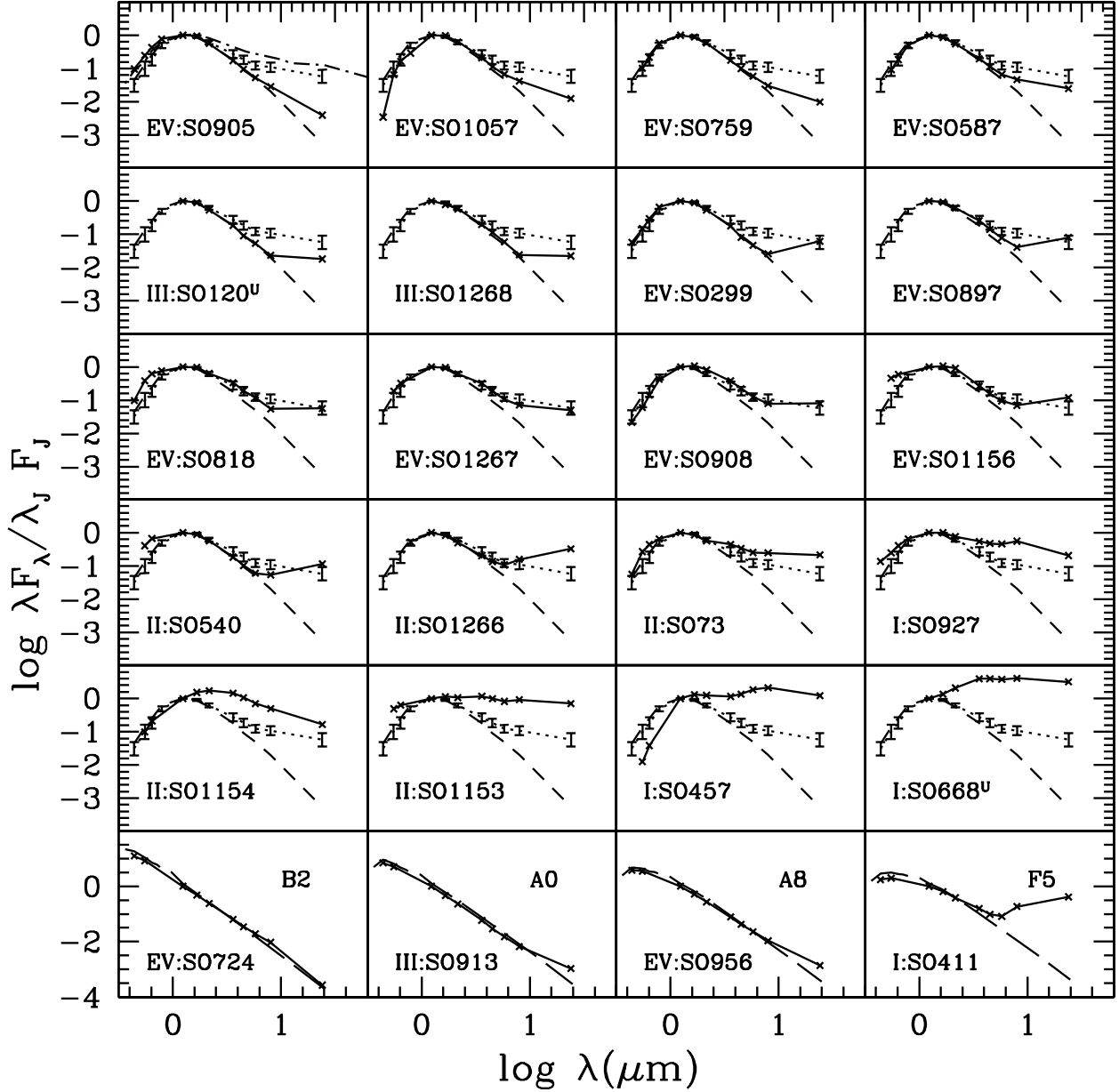


Fig. 13.— Spectral energy distributions for selected stars, illustrating the diversity of disks found in the  $\sigma$  Orionis Cluster. The first 5 rows show stars in the mass range of TTS. Dotted and dashed lines represent the median SED of optically thick disks and non-excess stars of the  $\sigma$  Orionis cluster, respectively. Error bars denote the quartiles of the optically thick disk median SED. Dot-dashed line, shown in the first panel, represents the median SED of optically thick disks in Taurus. The last row shows stars in the mass range of HAeBe; these are compared with the photosphere of a star with a similar spectral type (long-dashed line; Kenyon & Hartmann 1995). Each panel is labeled with the internal running identification number and the classification from §4.2.

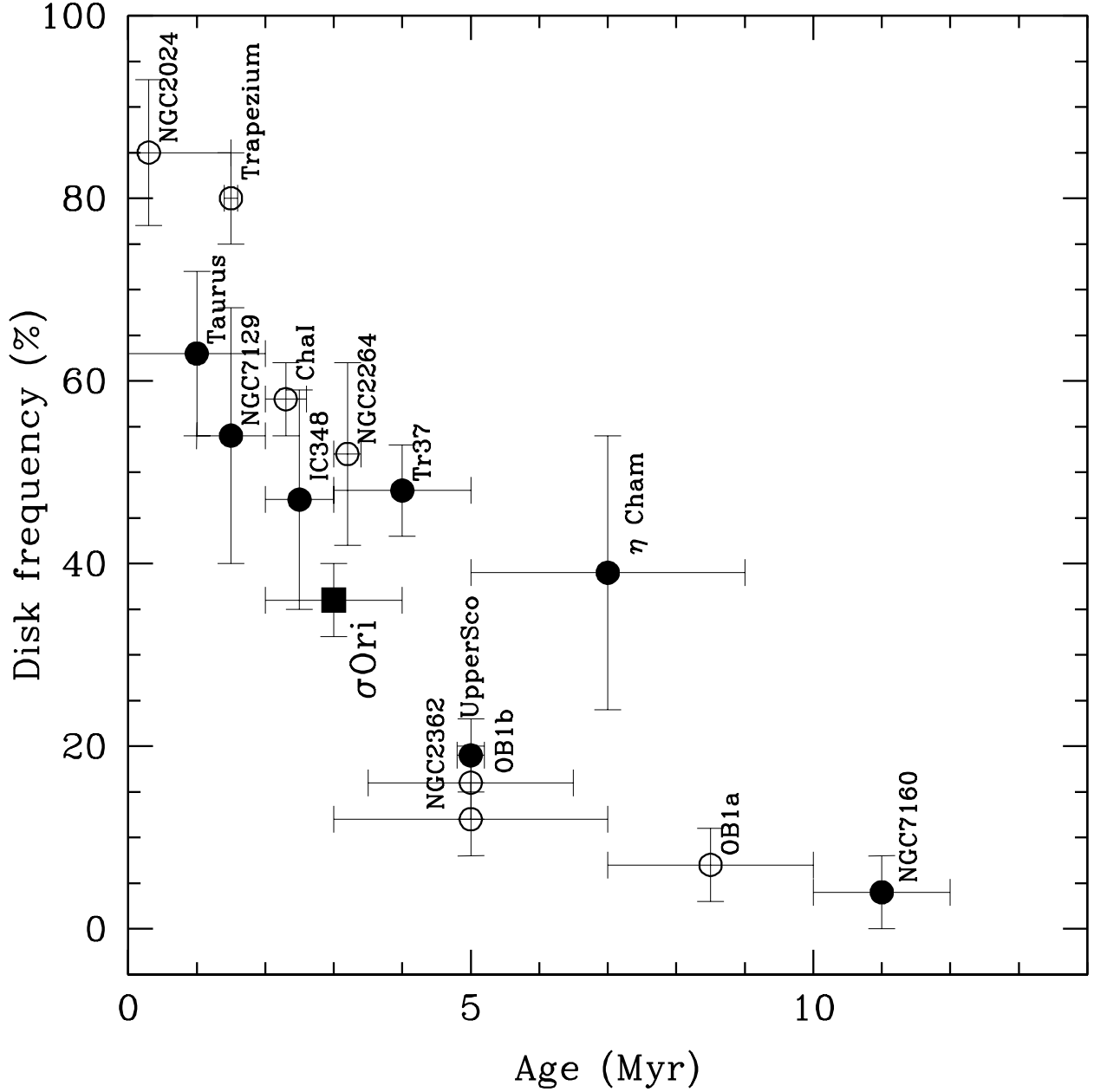


Fig. 14.— Fraction of stars with near-infrared disk emission as a function of the age of the stellar group. Open circles represent the disk frequency for stars in the TTS mass range, derived using JHKL observations: NGC2024, Trapezium, NGC2264 and NGC2362 from Haisch et al. (2001), Chamaleon I from Gómez & Kenyon (2001), and OB1a and OB1b sub-associations from Hernández et al. (2005). Solid symbols represent the disk frequency calculated for stars in the TTS mass range using IRAC data: Taurus (Hartmann et al. 2005c), NGC7129 (Gutermuth et al. 2004), IC348 (Lada et al. 2006), Tr 37 and NGC7160 (Sicilia-Aguilar et al. 2006), Upper Scorpius (Carpenter et al. 2006),  $\eta$  Chameleontis (Megeath et al. 2005a) and  $\sigma$  Orionis cluster (this work)

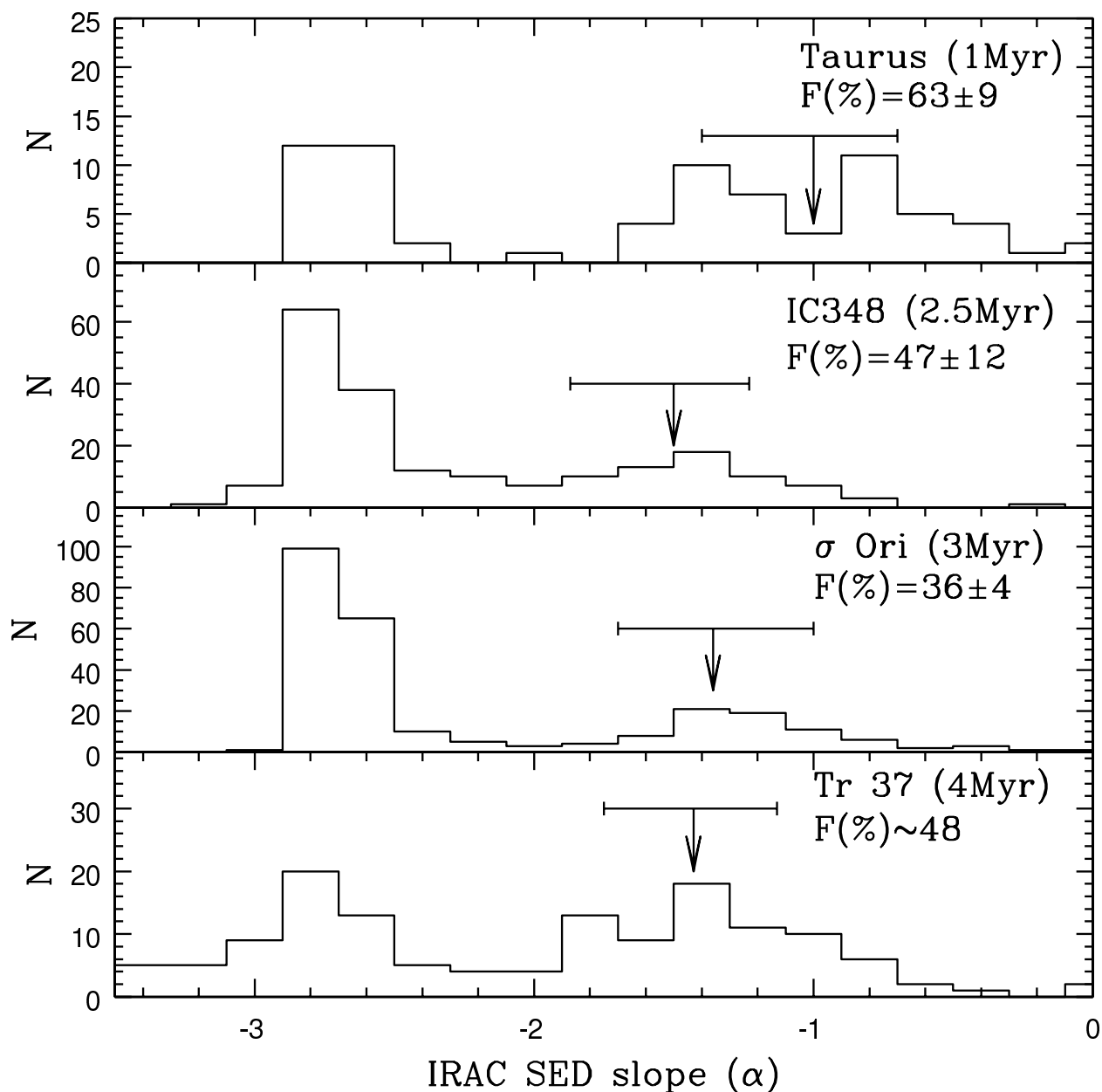


Fig. 15.— IRAC SED slope distribution for young stellar groups with differing ages. The dotted line defines the limit between thick disks and evolved disks. Fractions of disk-bearing stars and stellar ages are included in each panel: Taurus (Hartmann et al. 2005c), IC348 (Lada et al. 2006),  $\sigma$  Orionis (this work) and Tr 37 (Sicilia-Aguilar et al. 2006). The median of  $\alpha$  slope and its quartiles for disk-bearing stars in each stellar group are indicated with arrows and error bars, respectively.

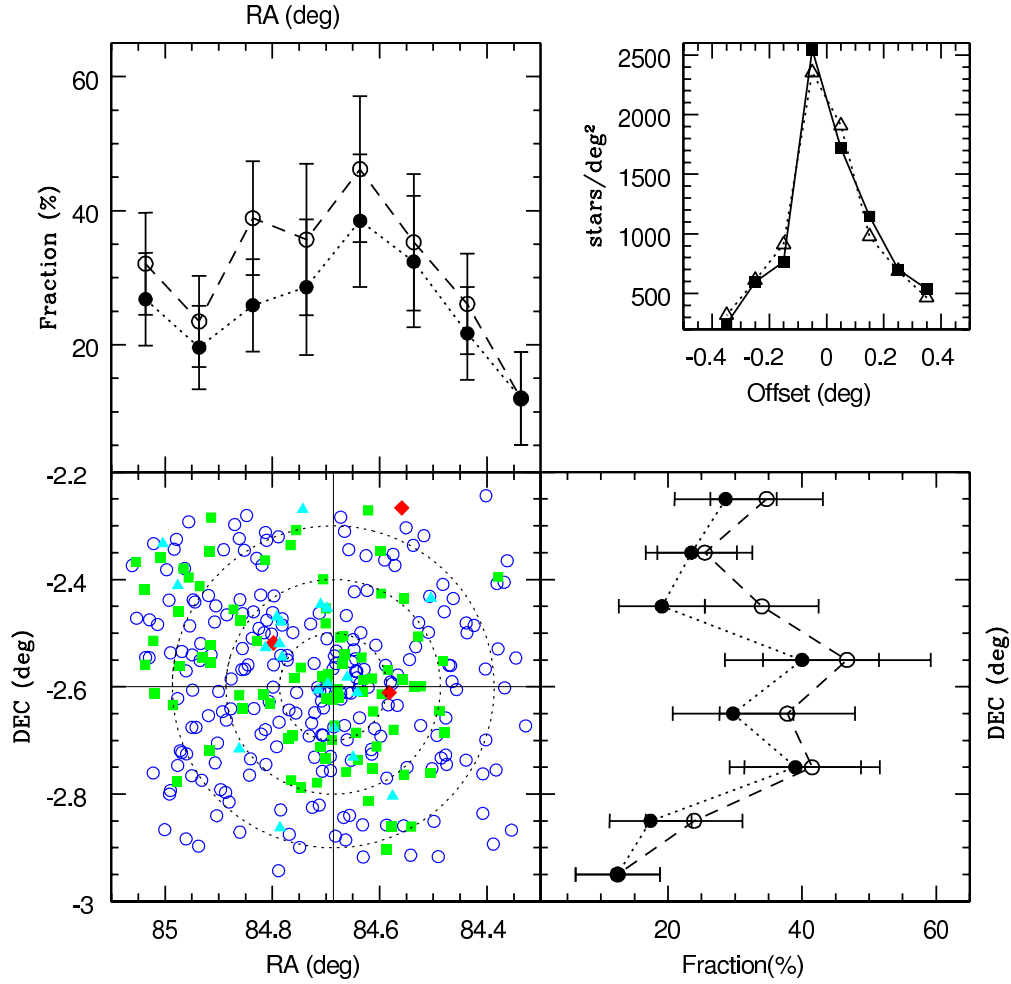


Fig. 16.— Diagrams illustrating the space distribution of members, disk fractions and the density of the cluster. The lower-left panel shows the location of members in the  $\sigma$  Orionis cluster. Symbols are similar to Figure 8. Dotted circles define radial distances (at 0.1, 0.2 and 0.3 degree) from the center of the cluster and solid lines define the semi-circles East-West (vertical) and North-South (horizontal) used to calculate the fraction of disks in bins at several radial distance from the star  $\sigma$  Ori. Upper left panel shows the fraction of thick disk stars (filled circles + dotted line) and disk-bearing stars (open circles + dashed line) in radial distance bins defined by the semicircles East-West. Similarly, lower-right panel shows the fraction of disks in radial distance bins defined by the semicircles North-South. Upper-right panel shows the density of members in radial distance bins defined by the semicircles East-West (filled squares+solid line) and by the semicircles North-South (open triangles+dotted line) [See electronic edition of the journal for a color version of this Figure]

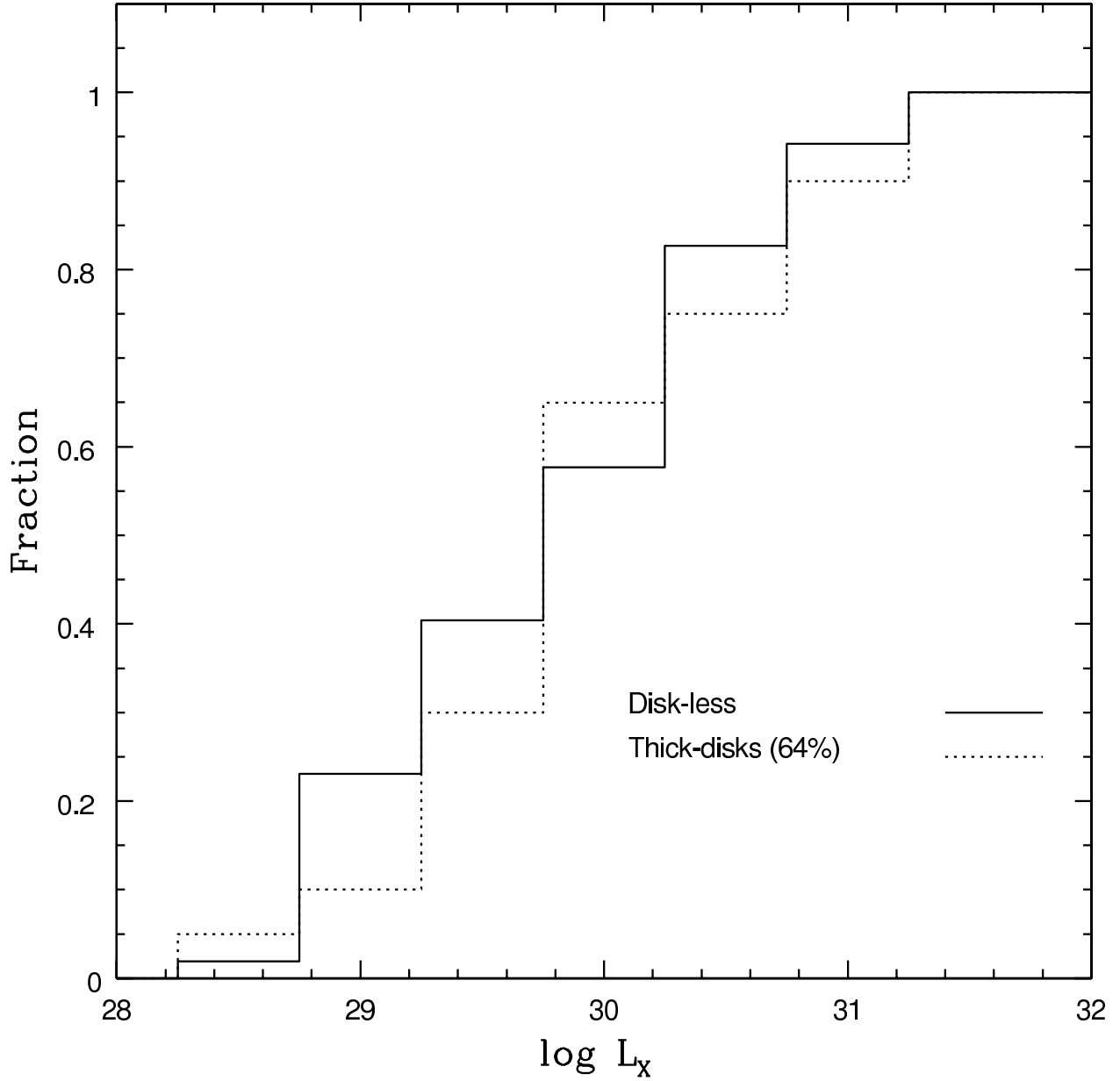


Fig. 17.— Cumulative distribution of non-excess stars and optically thick disk stars as a function of X-ray luminosity. A Kolmogorov-Smirnov (KS) test shows a significance level of 64% when comparing both populations. This suggests that the X-ray emission has a similar origin in non-excess stars (like WTTS) and stars with optically thick disks (like CTTS)